ASSESSING THE IMPACT OF BUFFER SALT CHOICE ON THE FORMATION OF DNA I-MOTIFS

by

Caroline West

A thesis submitted to the faculty of
The University of North Carolina at Charlotte
in partial fulfillment of the requirements
for the degree of Master of Science in
Chemistry

Charlotte

2023

Approved by:

_____
Dr. Joanna Krueger

_____
Dr. Juan Vivero-Escoto

_____
Dr. Brian T. Cooper

_____
Dr. M. Brittany Johnson

ABSTRACT

CAROLINE MECHELE WEST. Assessing the Impact of Buffer Salt Choice on the Formation of DNA I-Motifs.
(Under the direction of DR. JOANNA KRUEGER)

I-motifs are intercalated cytosine quadruplexes discovered in 1993, but they weren't shown to exist in the cell nucleus until 2018. While their biological role has yet to be fully elucidated, they have been implicated in regulating expression of several genes involved in cancer, depression, diabetes, neurodegenerative diseases, and cardiovascular disease. The effect of monovalent cations on i-motif formation has been the subject of numerous reports with inconsistent results. The most notable of these discrepancies are contradictory reports of sodium and lithium ions stabilizing or destabilizing i-motifs. These inconsistencies could be due to the use of different buffer salts in these studies. The RAD17 promoter sequence has been reported to form i-motif structures at physiological pH and has been used as a model system to study potential interactions of buffer systems with DNA. Confirmation of i-motif formation was demonstrated with circular dichroism (CD) which can distinguish between various DNA secondary structures due to unique spectral signatures associated with the orientation of the nucleotide bases in solution. Small Angle X-Ray Scattering (SAXS) was utilized to provide additional information to validate structural assumptions from CD. Despite previous studies touting the stability of RAD17 as an i-motif, RAD17 only appeared to have formed i-motifs in HEPES buffer at pH 7.4, but not in buffers containing Tris at the same pH. Herein we demonstrated that differences in metal ion concentrations induce different structural changes to RAD17 depending on buffer selection.[1-3]

ACKNOWLEDGEMENTS

I would like to express my deepest appreciation to the UNC Charlotte Chemistry Department for supporting my academic and research endeavors from my start at the UNC Charlotte in Summer 2019 as a Post-Baccalaureate student through the Master's Degree Program process.

Specifically, I would like to first thank Dr. Joanna Krueger for her mentorship and support. I learned a substantial amount of lab techniques under her guidance, which helped develop my skillset as a scientist. Her support of women in science was instrumental in my ability to succeed in the program.

Next, I would like to thank my committee members Dr. Juan Vivero-Escoto, Dr. Brian Cooper, and Dr. M. Brittany Johnson for their valuable experience and insight. They have been very supportive throughout this process, and their feedback greatly improved the quality of my research.

Other UNC faculty I would like to thank include Dr. Jerry Troutman for his mentorship throughout the degree process and helping me navigate the logistics. I would also like to thank Dr. Irina Nesmelova at UNC Charlotte for allowing us access to the Jasco 1500 CD Spectrophotometer and Dr. Richard Dudley for his assistance with the Jasco 1500 CD Spectrophotometer. Dr. Thomas Schmedake was instrumental in helping with acquiring the lab supplies necessary to conduct the experiments in this thesis.

Furthermore, Brenda Fandrey and Cindy Honegger in the stockroom were immensely helpful in ensure I had the materials I needed to be successful.

I would also like to thank Dr. Lewis A. Rolband for his assistance in developing protocols and data analysis.

I would like to thank Kathryn Burnett from the Advanced Light Source (ALS), a national user facility operated by Lawrence Berkeley National Laboratory on behalf of the Department of Energy, Office of Basic Energy Sciences, through the Integrated Diffraction Analysis Technologies (IDAT) program, supported by DOE Office of Biological and Environmental Research. Additional support comes from the National Institute of Health project ALS-ENABLE (P30 GM124169) and a High-End Instrumentation Grant S10OD018483. This advanced light source, specifically the SIBYLS Beamline was used for all the small-angle x-ray scattering data collection.

DEDICATION

I would like to dedicate this thesis to my two daughters, Arya and Josephine. Their love motivates me to continue to improve myself as a scientist so I can be a role model for them as a woman in science. They already are immensely curious about science, and that inspires me to continue working diligently to improve my research skillset.

TABLE OF CONTENTS

LIST OF TABLES

LIST OF FIGURES

LIST OF ABBREVIATIONS

ADF	Artificial Duodenal Fluid
AGF	Artificial Gastric Fluid
AIF	Artificial Intestinal Fluid
BCL2	B-cell lymphoma
C-myc	Cellular Myelocytomatosis
CD	Circular Dichroism
DNA	Deoxyribonucleic acid
FITC	Fluorescein Isothiocyanate
FRET	Fluorescence Resonance Energy Transfer
G1	Growth 1 Phase
GI	Gastrointestinal
HEPES	N-2-hydroxyethylpiperazine-N'2-ethanesulfonic acid
HT	High Tension
i-motif	Intercalated Motif
MES	2-Morpholinoethanesulphonic acid
N3	Nitrogen in the third position
nm	Nanometer
NUPACK	Nucleic Acid Package
^{o}C	Degrees Celsius
PAGE	Polyacrylamide gel electrophoresis
PBS	Phosphate Buffered Saline
PEM	Photoelastic Modulator
PTK7	Protein Tyrosine Kinase
Rg	Radius of Gyration
S1	Synthesis phase of cell cycle
SAXS	Small Angle x-ray Scattering
TAE	Tris Acetate EDTA
TB	Tris Borate
μM	Micromolar

CHAPTER 1: INTRODUCTION

1.1 I-motif Structure

Intercalated DNA motifs (i-motifs), also called cytosine quadruplexes, are four-stranded DNA structures that involve cytosine-cytosine base pairing. These structures are commonly found in promoter regions, telomers and the nucleus of cells, and they may play a role in transcription as well as gene expression. The "I" comes from "intercalated" due to the intercalated structure they exhibit of the cytosine pairing through each other. An illustration of their structures are shown in **Figure 1.1** below.[7]

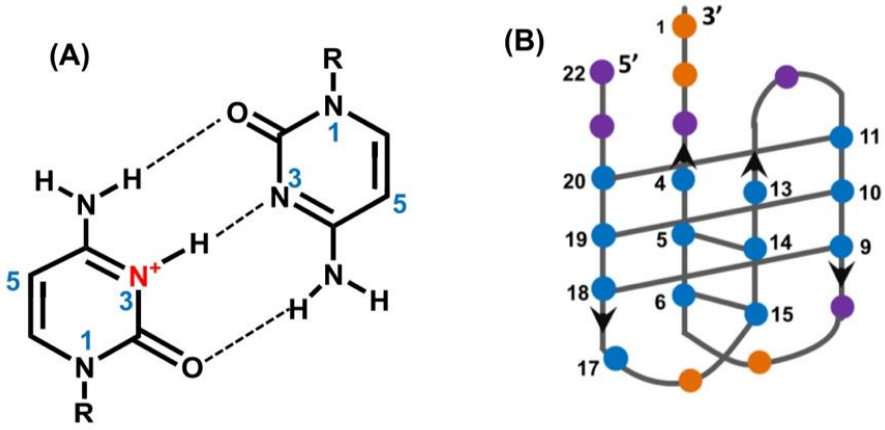

Figure 1.1: (A) Hydrogen bonding interaction of hemi protonated cytosine-cytosine base pairing. (B). Schematic of i-motif intercalated structure where the different colored dots represent different bases with blue for cytosine, purple for thiamine, and orange for adenine. Reprinted with permission from Paul, S[8]. Copyright 2020 American Chemical Society.

I-motifs were first discovered *in vitro* in 1993, but it was not until 2018 that they were found to exist naturally in living cells[9]. They remained elusive for so long because they are only found at the end of the G1 and start of the S1 phase of the cell cycle, which is a small portion of the cell's lifespan.[10] I-motifs also tend to occur in acidic environments rather than physiological pH, around 7.4, since this allows cytosine to become protonated at the N3 endocyclic nitrogen,

which then lends itself to hydrogen bonding with another cytosine. When the cytosines are paired, the proton does not stay with the original cytosine, but instead oscillates between the two cytosines.[11] I-motifs are usually transient structures and tend to be less stable than typical B-DNA because of the electrostatic repulsion of the phosphate backbones, which are in closer proximity. Another factor contributing to the lower stability of i-motifs is that there is a loss of π - π stacking interactions due to the bases having a different orientation in this particular quadruplex structure.

Despite the different factors that affect the stability of i-motifs, there are several methods reported in the literature to stabilize these structures. One of the most common ways to encourage i-motif formation, aside from lowering the pH of the surrounding media, is to simulate the molecular crowding environment of the nucleus with the addition of polyethylene glycol.[7, 12] Generally, longer sequences containing cytosine tend to be more stable; however, the exception is the "4n-1" rule that predicts greater stability to sequences that contain 4n-1 cytosines even at shorter lengths.[13] In this equation, n refers to the number of cytosines in a linear sequence. It is generally accepted that silver ions also help to stabilize i-motifs, but there is very little consensus on the effects of other cations on i-motifs, most notably lithium, potassium, and sodium.[14] Depending on the study, these cations either stabilize, de-stabilize, or have no effect on i-motif structure.

1.2: Applications of I-Motif Technology

Initially, i-motifs were utilized for nanotechnology to act as a pH dependent switch in a variety of applications for therapeutic and diagnostic purposes. Now i-motifs serve as critical design elements in devices performing a variety of functions from DNA logic systems, switchable DNA origami, and many nanoscale platforms.[15] I-motifs are frequently used in cancer treatment

because their pH dependence allows them to selectively target cancer cells due to the acidic tumor micro-environment. One research group created a treatment they called the "Molecule Doctor" (pH-Apt-MD), which uses a novel aptamer that facilitates pH dependent drug release and has activatable fluorescence when it is located in the presence of cancer cells.[16]

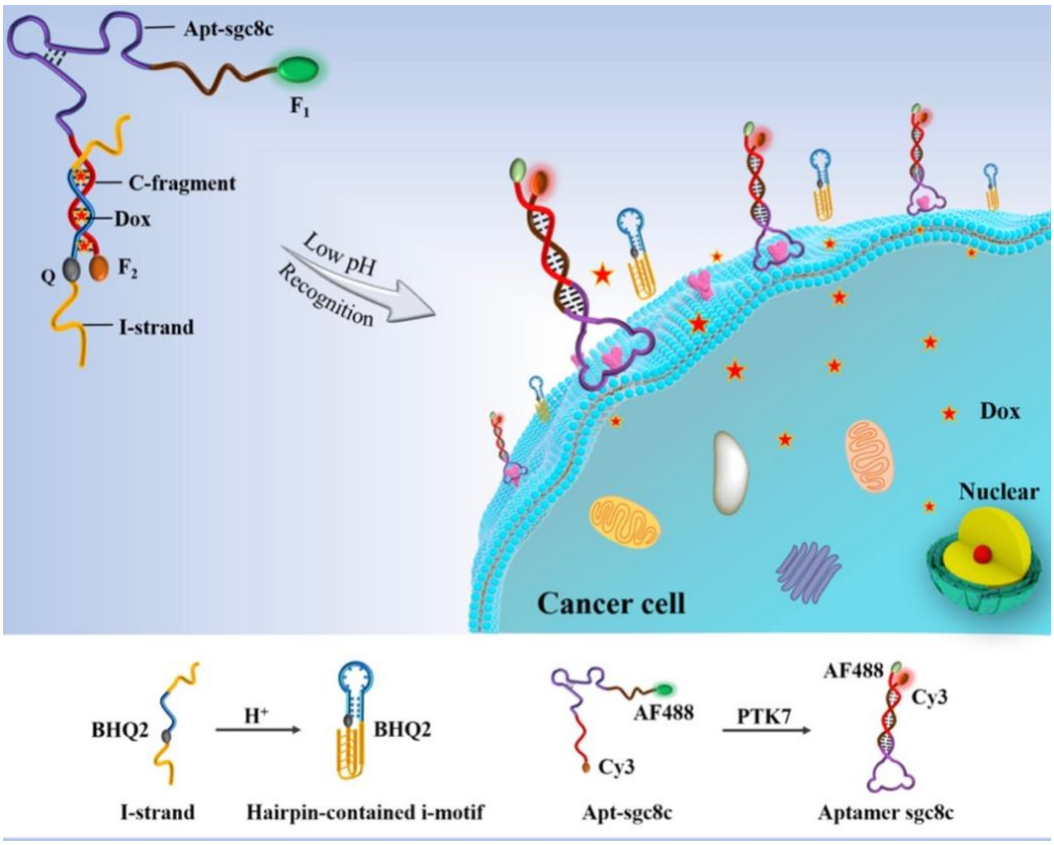

Figure 1.2: This schematic shows how pH-Apt-MD changes its configuration based on its environment to provide targeted delivery and imaging. Reprinted with permission from Ma, W. *et al* 2021. Copyright 2021 American Chemical Society.[16]

At physiological pH, the molecule consists of a DNA strand with an aptamer that recognizes specific tumor cells, an "I strand" that has the potential to form an i-motif along with a hairpin, two fluorophores, and a quencher (**Figure 1.2)**. At a neutral pH, doxorubicin is inside the double stranded region of the synthetic DNA structure, and only one of the fluorophores produces

a fluorescent signal due to the proximity of the quencher to the other fluorophore. When the molecule recognizes protein tyrosine kinase (PTK7) on the surface of a cancer cell, the acidic tumor microenvironment triggers re-arrangement of the molecule when it attaches to the surface. The re-arrangement leads to two structures, one with the quencher contained within a hairpin/i-motif, and the other one containing the aptamer with the affinity to the cancer cells as well as the two fluorophores. This causes a strong fluorescent signal from the aptamers bound to the cancer cell to aid in its visualization. Moreover, as a consequence of this re-arrangement, doxorubicin is simultaneously released to treat the cancer cell. They found that utilizing the i-motif was critical to reducing background noise because it only allows the strong fluorescent signal when exposed to a pH of 6.5 and below, which is common around cancer cells.[16]

Another example of current applications of i-motif technology was presented by Hu *et al* (2022) in the form of a DNA hydrogel that combined A-motifs and i-motifs in a system designed to facilitate oral insulin delivery.[17] A-motifs are a double helix structure characterized by adenine-adenine base pairing, and they are stable at pH values 1.2 to 3.0.[17] Diabetic compliance with an insulin regimen is a long-standing issue due to the inconvenience of self-administered subcutaneous insulin injections. Compliance improves with oral administration, but oral insulin easily degrades in the acidic GI tract, and less than 1% of the administered dosage survives to modulate blood sugar levels. A potential solution to this problem is to use DNA and its numerous structural configurations to modulate nanoparticle properties to allow insulin to travel through the GI tract and reach its target intact. Previous attempts at utilizing i-motifs for insulin delivery worked well down to a pH of 5.0 because that is when cytosines can be protonated to form quadruplexes, but failed at more acidic conditions. This paper particularly looks at a pH responsive DNA hydrogel that works by incorporating A-motifs and i-motifs to accommodate a wider pH

range from 1.2 to 6.0. This system then releases insulin at the physiological pH. This "smart" hydrogel is a solid polymer cross-linked with A-motifs and i-motifs that contains insulin in its matrix, so when the A-motifs and i-motifs dissociate, the bridges cross-linking the solution are broken. A schematic showing the DNA structural changes associated with the hydrogel traversing the GI tract in response to pH changes is illustrated in **Figure 1.3**. When this happens, the polymer dissociates, thereby releasing the insulin. Utilizing this design, the hydrogel can deliver its contents to the small intestine successfully.

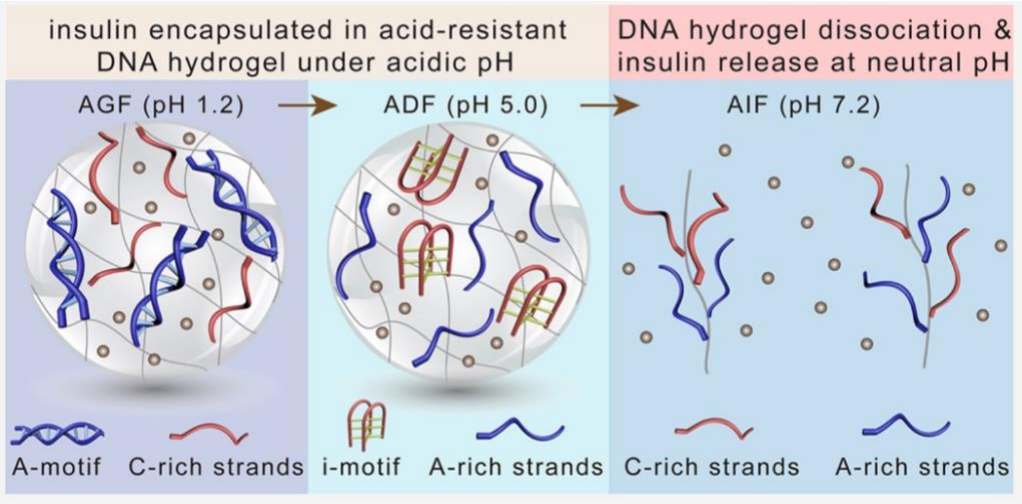

Figure 1.3: Schematic illustrating how the unique DNA hydrogel technology is able to survive the gastrointestinal tract to facilitate oral insulin administration while retaining a high degree of bioavailability. Reprinted with permission from Hu *et al* 2022. Copyright 2022 American Chemical Society.[17]

Circular dichroism (CD) was used to verify A-motif and i-motif formation. A-motifs were shown at a pH from 1.2 to 3.0, and i-motifs at a pH of 4.0 to 6.0. This is illustrated by the dark grey lines of the gel in the artificial gastric fluid (AGF) and the A-motifs that are keeping the gel cohesive at a pH of 1.2. The gel matrix is also stable in the second panel due to the i-motif stability at pH 5.0. However, once in the artificial intestinal fluid (AIF), the gel matrix is destabilized as neither i-motifs nor A-motifs are generally stable at a pH of 7.2. To verify the release of insulin, the researchers used UV-Vis spectroscopy and labeled the insulin with fluorescein isothiocyanate

(FITC). FITC absorbs light at 450 - 500 nm, which would be distinct from DNA that absorbs at 260 nm. They found that insulin was completely released from the hydrogel when in the artificial intestinal fluid after one hour. Only three to four percent of the insulin was released from the polymer in the artificial gastric and duodenal fluid. In addition to the pH dependent formation of A and i-motifs, the authors theorized that the insulin was contained in the polymer because below 5.0 pH, insulin is positively charged, so it has a favorable electrostatic interaction with DNA. On the contrary, at 7.2 pH, insulin is negatively charged, causing electrostatic repulsion. Overall, this novel platform for oral insulin administration shows promise for improving diabetes management due to the properties of i-motifs and A-motifs.

1.3 Role of i-motif is transcriptional regulation

Even though there are several applications of i-motifs in biotechnology, the question still exists as to what role i-motifs play in regulating body processes. The discovery of i-motifs existing in living cells was a pivotal moment for i-motif research because it showed that i-motifs are more than merely a laboratory oddity. This discovery was made possible through the isolation and identification of an antibody, called “i-Mab” by the researchers who discovered it, that binds selectively to i-motifs.[9]

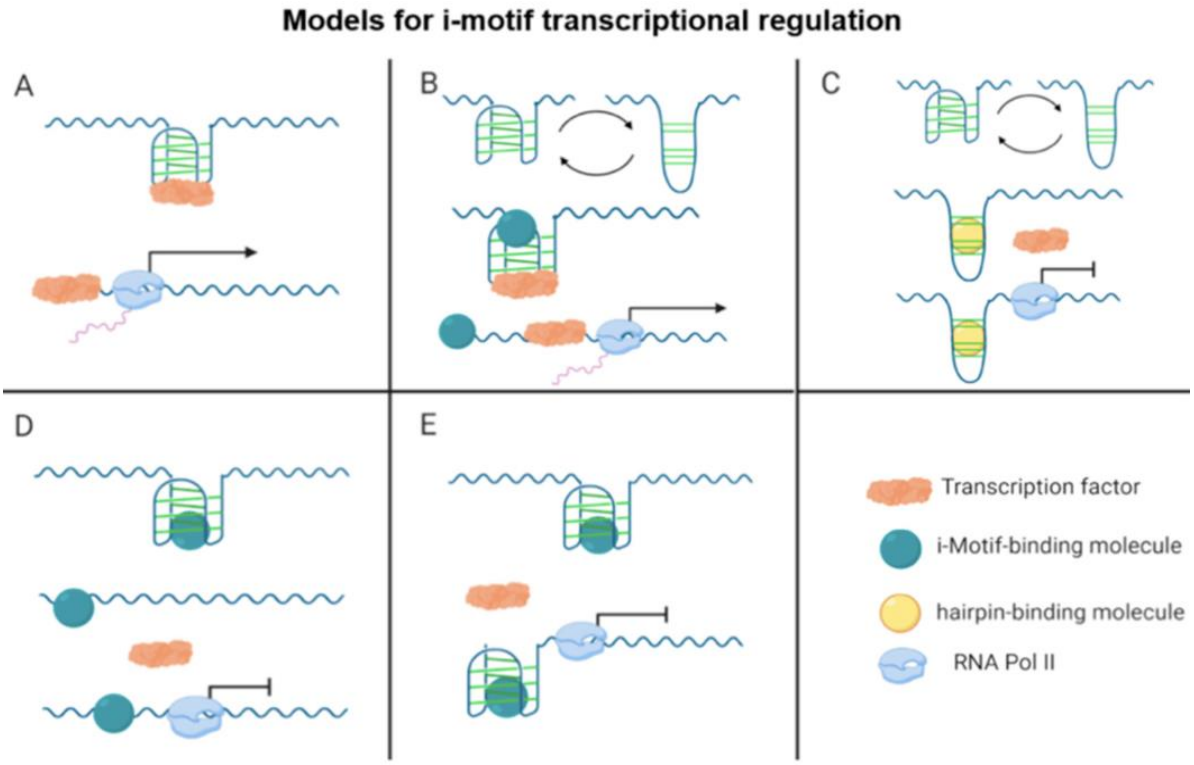

Figure 1.4: Five potential models that illustrate how i-motifs could be involved in transcriptional regulation. The complete arrows in A and B indicate DNA structures promoting transcription, whereas the truncated arrows in C, D, and E show DNA structures preventing transcription. Reprinted with permission from Brown, S *et al* 2021[18] under the Creative Commons Attribution (CC BY) license (https://creativecommons.org/licenses/by/4.0/).

It is largely thought that i-motifs assist with transcriptional regulation due to their prevalence in promoter regions. The current theorized models of how this regulation occurs are summarized in **Figure 1.4**.[18] The reason behind the multiple potential models is that in some genes, such as c-myc, the presence of i-motifs can lead to reduced transcription, whereas in other genes such as BCL2, i-motifs cause an increase in transcription.[18] The BCL2 (B-cell lymphoma-2) codes for the BCL2 protein which can inhibit apoptosis, so the upregulation of this protein promotes cancer.[19] C-myc is a transcription factor and induces greater transcription for other tumor promoting factors such as increased angiogenesis.[20] The gene dependent nature of i-motifs upregulating or downregulating transcription is an area of significant research currently due to the ambiguity of how transcription may be regulated with this structure. In **Figure 1.4**, panels A and

B are illustrating how i-motifs may upregulate gene expression by binding to the transcription factor, allowing transcription to occur. Panels C, D, and E are illustrating possible mechanisms of transcriptional repression. The mechanism shown in C is unique in that it shows the dynamic equilibrium between hairpins and i-motifs. D and E both include a molecule that binds to i-motifs, adding to its stability, and thus preventing the transcription factor from binding, leading to reduced transcription. Due to the current lack of understanding, it is unclear which mechanism is occurring, and it is likely that more than one of the mechanisms could be correct depending on the gene of interest.

1.4: Impact of ions on i-motif stability

I-motif stability is greatly affected by ion concentration and identity, but there are discrepancies in the literature as to which ions stabilize or destabilize i-motifs, and what concentrations may induce these effects. For a summary of these effects, see **Table 1.1**.

Table 1.1: Brief summary of effect of cations on i-motif stability. Definitions: SSC (saline sodium citrate buffer), SCB (sodium cacodylate buffer), PB (phosphate buffer), MeCN (acetonitrile).

Cation	Buffer	Effect on i-Motif
Sodium	HEPES[21]	Stabilizes
	SCB[22], *MeCN[23], *Computational[24], MES[25]	De-stabilizes
Lithium	MES[3, 26]	Stabilizes
	SCB[22]	No effect
	HEPES[21], *MeCN[23], *Computational[24]	De-stabilizes
Potassium	HEPES[21], PB[27], SSC[27], SCB[27]	Stabilizes
	MES[3, 25-27], Bis-Tris[27]	De-stabilizes
	SCB[22]	No effect
Magnesium	SCB[28]	Stabilizes
	SCB[22]	No effect
Calcium	SCB[28]	Stabilizes
	SCB[22]	No effect
Silver	SCB[14], *MeCN[23], PBS[29, 30], *Computational[24]	Stabilizes
Copper	*MeCN[23], *Computational[24]	Stabilizes
	SCB[31]	De-stabilizes
Gold	*Computational[24], HEPES[32]	Stabilizes

*No buffer present

One apparent issue that may be contributing to these contradictory findings is different buffer choice between researchers. Very few of the papers in the literature included why they chose a particular buffer system or acknowledged any potential interactions between the i-motif and the composition of the solution their DNA was suspended in. what is being studied, thoughtful buffer

choice is critical to making valid conclusions. However, given the contradictions present in **Table 1.1**, there are other factors in the experimental setup leading to different conclusions how ions impact DNA secondary structure. For sodium, lithium, and potassium in particular, the researchers using different buffer systems reported different effects as to how these ions are stabilizing, de-stabilizing or exhibiting no effect on i-motifs. There are several other factors that could be contributing to these different findings such as using molecular crowding agents, ion concentration used to titrate the buffer to the correct pH is not always reported, temperature, different oligonucleotide sequences, and variations in pH. Mostly i-motif studies are conducted at a slightly acidic pH, but this is not always consistent.[7] Despite the many potential sources of experimental variation, starting with exploring the buffer interactions is a reasonable approach to start improving the quality and reproducibility of i-motif research.

Studies involving cytosine-cytosine base pairing without being part of an oligonucleotide sequence or in a buffer system provides an intriguing contrast the majority of the literature on i-motifs. Gao *et al* 2016 created cytosine metal solutions in acetonitrile to better understand what is happening structurally with i-motifs utilizing infrared multiphoton dissociation (IRMPD) and density functional theory, which is computational.[23] Their proposed mechanism shown in **Figure 1.5** illustrates that the N3 nitrogen of the cytosines is coordinating to the metal ion. In true i-motifs, the hydrogen bonding of the N3 nitrogen is critical to stability.[23]

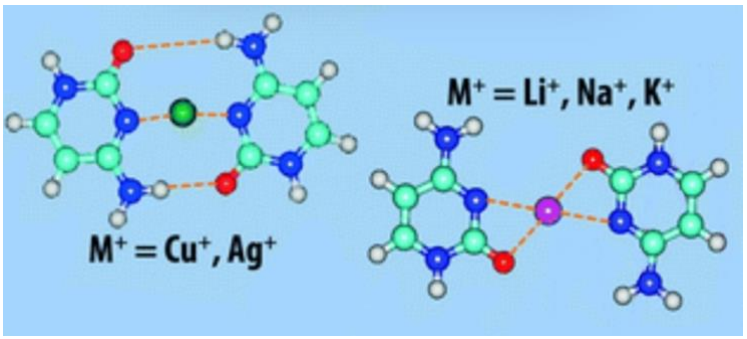

Figure 1.5: Model of cytosine-cytosine base pairing with transition metals compared to alkali metals. The schematic shows that transition metals form more stable i-motif like structures than alkali metals. The key is as follows: Red: oxygen, white: hydrogen, blue: nitrogen, green: transition metal, purple: alkali metal. Reprinted with permission from Gao 2016 under the Creative Commons Attribution (CC BY) license (https://creativecommons.org/licenses/by/3.0/).[23]

The key findings in the studies looking at cytosine bases in isolation from an oligonucleotide sequence were that transition metals binds differently to cytosines than alkali metals. Cytosine acts as a monodentate ligand for transition metals with a covalent-like bond with the N3 nitrogen on the cytosine.[23] This follows the hard-soft acid-base (HSAB) theory that cytosine is considered a soft base, and transition metals such as copper and silver are soft acids.[23] This is contrasted to the cytosine bidentate binding of alkali metals to the N3 nitrogen as well as the oxygen on the cytosine in a more ionic fashion.[23, 24] These differences lead to transition metals forming a more ordered, stable i-motif like structure, whereas alkali metals lead to de-stabilization of the i-motif structure.[23, 24] Interestingly, the conclusions from these studies are validated by crystal models of DNA structures forming dative bonds with silver.[33]

Single molecule FRET (fluorescence resonance energy transfer) was another way found in the literature to study how ions interact with i-motifs. Kim *et a*l 2014 found that in MES lithium led to de-stabilization whereas sodium and potassium stabilized i-motifs (**Figure 1.6**).[21]

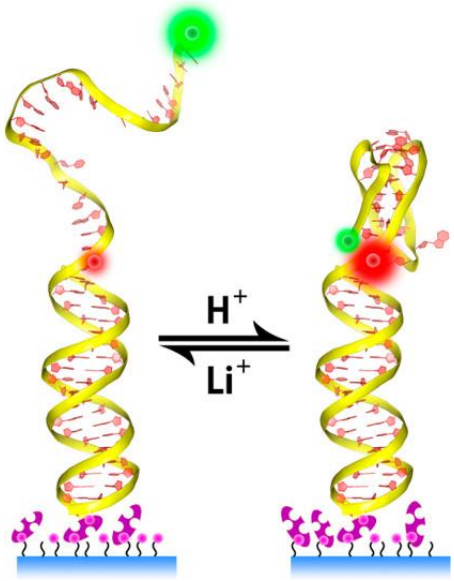

Figure 1.6: Schematic illustrating de-stabilization of the i-motif structure in the presence of lithium and folding of DNA into an i-motif in the absence of lithium based on FRET analysis. Reprinted with permission from Kim *et al* 2014. Copyright 2014 American Chemical Society.[21]

The rationale presented in the paper as to why different cations are leading to different structural effects is based on size differences of the ions. The intercalation distance between the cytosines is 1.8 Å, but due to other local effects, the ionic radius should be less than 1 Å to be capable of getting into the intercalation space. Potassium and sodium have too large a radius to accommodate that size constraint, whereas lithium at 0.7 Å is able to disrupt the hydrogen bonding leading to de-stabilization of the i-motif structure.[21]

For the purpose of the work presented herein, sodium and lithium were the two chosen cations to study. Sodium is often used in biological experiments since it is present naturally *in vivo* which can aid in mimicking physiological conditions.[34, 35] As such, sodium is one of the more ubiquitous ions present in DNA experiments.[36] Relevant values for sodium ions *in vivo* include the extracellular concentration of around 135 mM, intracellular cytoplasmic concentration of 10.9 mM, and intracellular nucleus concentration of 10.4 mM.[37, 38] Lithium was chosen as another ion

to study because it is also a monovalent cation like sodium, but it is not studied as much due to its limited biological relevance. Endogenous lithium is present *in vivo* at a concentration around 0.27 μM [39], and when lithium is prescribed as a medication, the goal serum concentration is 0.6 mM to 1.2 mM.[40-42] Another study found that the intracellular concentration of lithium was 0.5 mM when cells were exposed to the therapeutic concentration of 1 mM lithium with the cell medium.[43] Lithium as a therapeutic is used in the treatment of various mental illnesses, and while it has been used for decades, the exact mechanism of action is unclear. It has a much narrower therapeutic range than other medications, so greater research into lithium effects on the body, such as on DNA, is warranted.[40, 41]

There are several different buffer systems used to study i-motifs. One of the more common buffers is sodium cacodylate as well as lithium cacodylate.[14, 27, 44, 45] However, since these consist of arsenic salts, it questions the biological relevance of using such buffers. Other buffers reported in the literature when examining i-motifs are Britton-Robinson Buffer (boric acid, acetic acid, phosphoric acid)[46], MES (2-Morpholinoethanesulphonic acid)[21, 27], and phosphate buffered saline (PBS)[45, 47]. The landmark paper that identified i-motifs in living cell nuclei utilized a Tris[9] buffer system, and since Tris-Borate is an industry standard in terms of buffer selection for biological samples, this is the first buffer chosen for further investigation in the present work. In order to understand potential impacts of borate in the system, tris acetate was the second buffer, and HEPES (N-2-hydroxyethylpiperazine-N'2-ethanesulfonic acid) was chosen as the third buffer due to the structural differences between HEPES and tris. The structure for the buffers used for this study are illustrated in **Figure 1.7**. The buffers were titrated to a pH of 7.4, since this is regarded as the physiological pH *in vivo*.[48] However, different intracellular components can have different pH values, and the pH of the nucleus is reported to be around 7.2.[49]

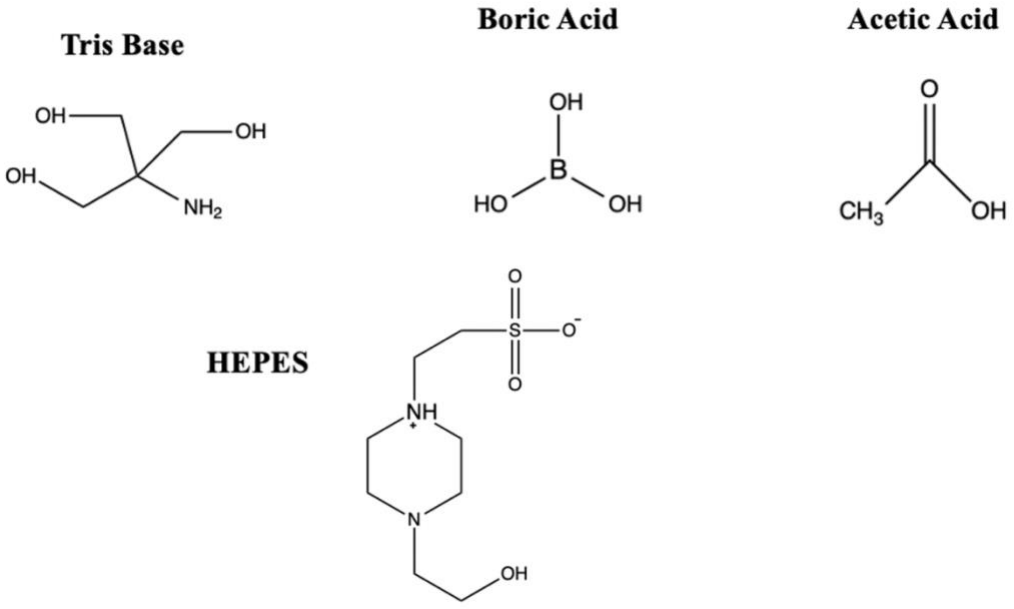

Figure 1.7: Structures of the buffers in their neutral state including Tris Borate, Tris-Acetate and HEPES buffers used. Images created with ChemDraw software.

1.5 RAD17 Promotor Sequence as a Model System

When DNA undergoes stress during replication the replication fork can stall or collapse which attracts certain proteins to the area, such as RAD17. These proteins prevent replication from occurring until the stress is resolved, which is vital to assisting with appropriate cell function. RAD17 is a cell checkpoint protein that is part of a complex that repairs double stranded breaks. A schematic of the mechanism by which RAD17 aids in DNA damage repair is shown in **Figure 1.8.** The promoter region of RAD17 is one of many DNA damage repair gene promotor regions that have been found to form i-motifs at physiologically relevant pH, giving it great potential as a model system for studying i-motif structural characteristics.[46] The relevant region of the promotor sequence of RAD17 is a 25-nucleotide sequence:

5’-CCACCCCCCCCCGCCCCCCCCCGGA

This sequence was found to form the most thermally stable i-motif of the 25 different DNA damage oligos tested at pH 6.9.[46] This makes it an ideal model system for investigating the formation of stable i-motifs in a variety of buffer conditions.

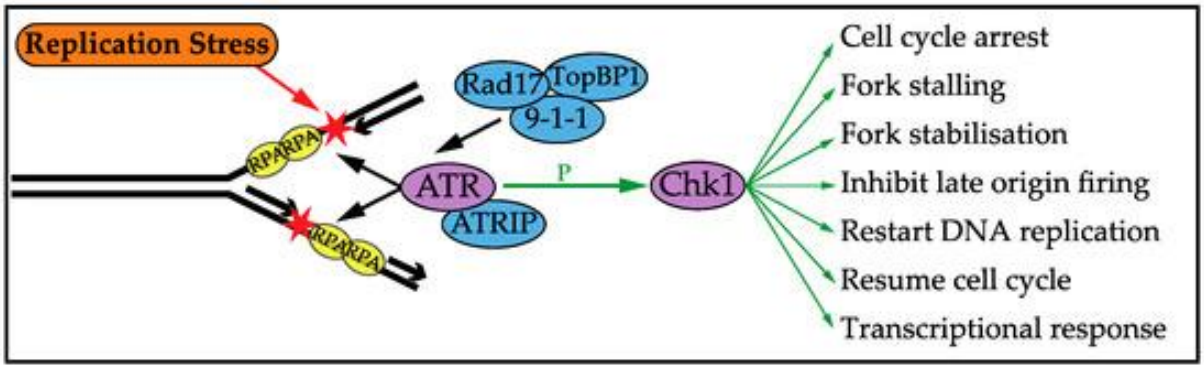

Figure 1.8: Schematic showing the role RAD17 plays in DNA damage repair. Prolonged exposed single-stranded DNA triggers the DNA damage response pathway, which starts with replication protein A, shown as RPA binding the single strand. RPA binding triggers recruitment of ATR (Ataxia Telangiectasia and Rad3-related protein) and ATRIP (ATR interacting protein) while also recruiting RAD17. These interactions lead to phosphorylation of Chk1 to initiate the DNA damage response mechanisms listed on the right side of the figure. Reprinted from Herlihy *et al* 2017[50] through Creative Commons Attribution (CC BY) license (https://creativecommons.org/licenses/by/4.0/).

1.6 Circular Dichroism

The current industry standard for assessing the presence of i-motifs or other DNA secondary structures is circular dichroism (CD) because it can quickly and relatively easily provide information on the predominant structure present in the sample.[51] It is anticipated that there are two main sources of chirality that give rise to the CD signal. First is the chirality of the nucleobase around the anomeric carbon. The second source is the DNA folding into various secondary structures such as hairpins, i-motifs, G quadruples, or triplexes.[52, 53] DNA secondary structure can be elucidated by CD because the nucleotides of the DNA act as the chromophore, absorbing UV light through **π -π*** transition.[54] It is important to note that sequence specific details cannot be ascertained, but merely the presence or absence of particular structures. Another important caveat

is that the CD signal arises from the predominant species present in the sample. For example, if 60% of the DNA in the sample is folded into an i-motif, while 40% of the DNA is folded into a hairpin, the spectra will tend to appear as an i-motif. This an important comparison because i-motifs are often found in equilibrium with hairpins and illustrates that not seeing a peak does not exclude a structure from being present, it's that other structures are not the predominant structure in the solution.[2, 52]

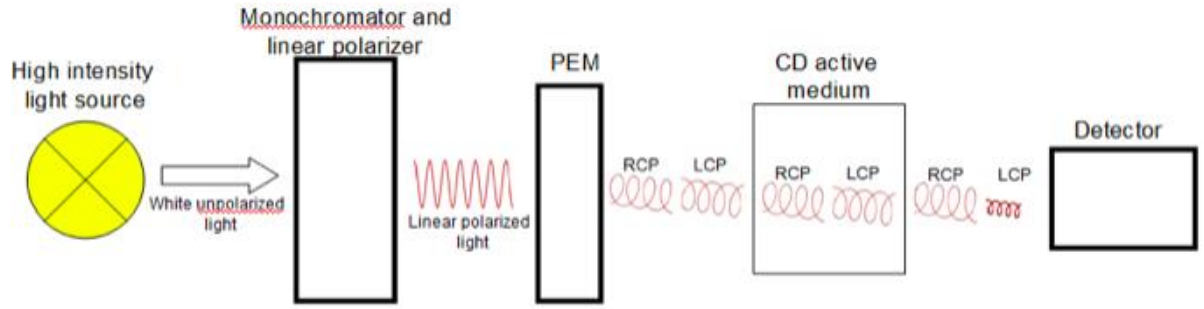

Figure 1.9: Diagram of a typical CD instrument. Reprinted with permission from Reference 9 under a CC BY 4.0 License (https://creativecommons.org/licenses/by/4.0/). [55]

The process from the light to obtaining data can be shown by a box diagram shown in **Figure 1.9**. CD involves a high intensity light source such as a xenon arc lamp where the light from the lamp passes through a linear polarizer so that the light is propagating through one plane. For this linearly polarized light to become circularly polarized, it must go through the photoelastic modulator (PEM). Birefringence is then achieved by stressing the quartz of the PEM by applying a 50 kHz frequency via the piezoelastic element. This causes the polarized light to refract into two light rays, with each one being circularly polarized in the opposite direction.[55]

This light then goes through the sample, and if the sample exhibits chirality or is in a chiral environment, there will be a difference in the absorbance of left versus the right circularly polarized light. This difference is what is analyzed to provide structural insights.[56]

Another aspect of CD is the High Tension (HT) Voltage component. The HT voltage is applied to the photomultiplier tube to increase the sensitivity of the detector, and changes its gain based on the amount of light coming out of the sample and hitting the detector. If too few photons are hitting the detector, the signal is amplified by increasing the gain and the HT voltage.[56]

When observing CD spectra, it is useful to compare the obtained curves to spectra of known structures. For the purpose of this research, the most significant spectral signature to be aware of is for i-motifs. However, since i-motifs are often in equilibrium with hairpins[2], it is useful to be aware of this structure as well to be better informed of potential structural changes, and these peaks are shown in **Figure 1.10**. I-motifs have the characteristic sharp peak at 290nm with an amplitude of 20 CD millidegrees (mdeg) or higher, and a negative peak around 265nm. Hairpins have a broader peak that is shifted to the left when compared to i-motifs, which have an amplitude of 10 mdeg or less.[2]

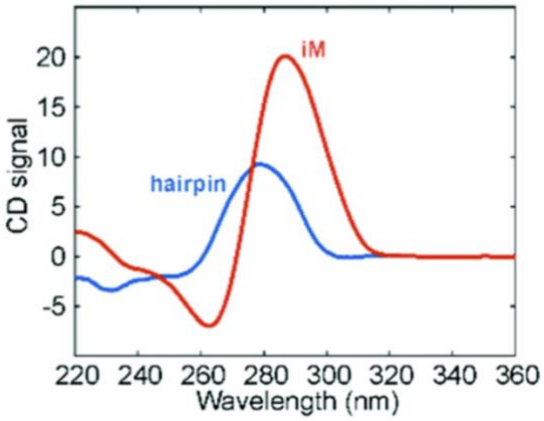

Figure 1.10: Circular dichroism spectra illustrating the peak differences in i-motifs versus hairpins from the literature. Reprinted with permission from Amato *et al* 2022 under the Creative Commons Attribution 3.0 (https://creativecommons.org/licenses/by/3.0/).[2]

If the DNA does not adopt a cohesive structure and instead exists as primarily disordered single stranded DNA, the spectra will closely follow the baseline without clearly defined peaks due to a lack of chirality, as shown in **Figure 1.11**.[27, 52]

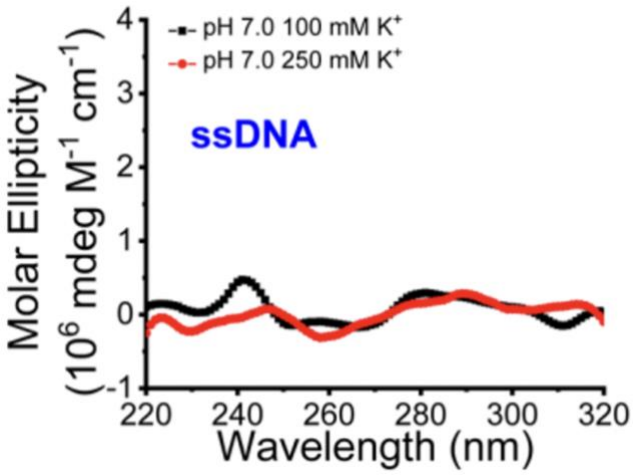

Figure 1.11: CD spectra from the literature comparing single stranded DNA structure in the presence of varying levels of potassium. It is included to indicate what the spectra looks like if the predominate structure is disordered single-stranded DNA. Reprinted with permission from Gao *et al*[27] through CC BY-NC-NC 4.0 DEED (https://creativecommons.org/licenses/by-nc-nd/4.0/).
57

1.7 Small Angle X-Ray Scattering

Small Angle X-Ray Scattering (SAXS) is a low resolution, solution-based technique that gives information about global structure, size, and shape of molecules.[58] The advantage SAXS has over higher resolution methods such as nuclear magnetic resonance (NMR) is that it can be used to study molecules in a dynamic environment and can probe flexibility. X-ray beams, typically from a synchrotron source, pass through the sample, and are scattered at an angle, 2θ.[57, 59, 60] The scattering vector, q, can be calculated from the angle at which scattered x-rays are observed considering the wavelength of the x-ray beam with the equation $q = 4\pi\sin\theta/\lambda$. This data is then plotted in a graph of intensity versus q.[57, 61] The particle size can be estimated using the radius of

gyration (*Rg*), which is a calculation of the root mean squared distance from every scattering volume in a particle to that particle's center of mass. The *Rg* can be found by looking at Guinier region of the I(*q*) graph which is at the low q or small angle area of the graph is located where the curve is linear[59, 61].

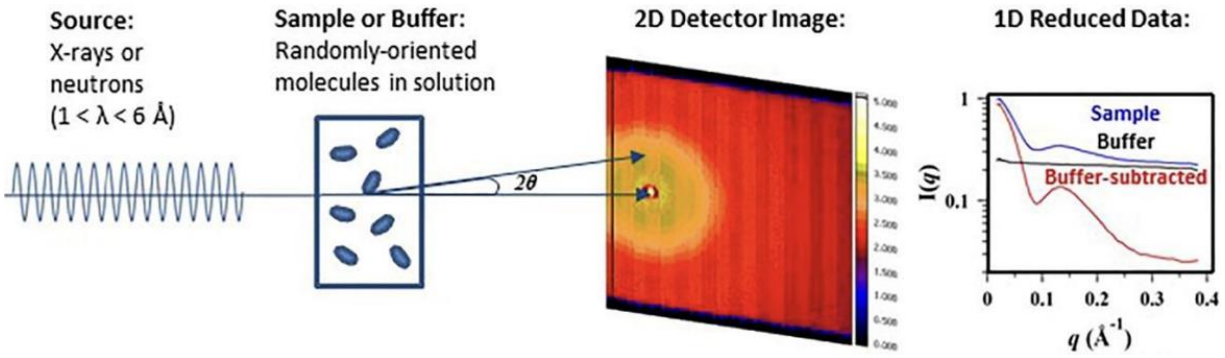

Figure 1.12: Schematic illustrating the process of obtaining data from SAXS and initial data computation. Reprinted with permission from Oliver *et al* 2019 under the Creative Commons Attribution (CC BY) license (https://creativecommons.org/licenses/by/4.0/).[59]

The way data is obtained and processed is shown in **Figure 1.12**. The 0 angle scattering intensity cannot be determined due to fundamental limitations, such as the inability to distinguish between forward scattered photons from the incident beam.[57] As a result, the intensity of the forward scattering at the 0 angle has to be estimated instead.[57] The significance of the figure showing the samples able to freely move in solution leads to random orientation is demonstrating how SAXS data is averaged over every possible orientation of the particle as it rotates.[61] There are several advantages obtaining structural information from particles in solution such as increased biological relevance and flexibility, but the random orientation of the particles reduces the possible resolution since the x-ray could hit the same particle at different orientations, leading to different scattering profiles that are then averaged.[57, 59, 62]

Eq. 1 $$\langle I(q) = \int |(\rho(r) - \rho_s)e^{iqr}dr|^2 \rangle$$

Equation 1 takes rotational average into consideration, as indicated by the brackets around the equation. This forms the basis of the first graph obtained from SAXS analysis by calculating intensity as a function of momentum transfer of SAXS data.[57]

The graph shown in **Figure 1.12** shows the initial data processing step of obtaining an Intensity (*I*) vs scattering vector (*q*) graph. The low q region is referred to as the Guinier region and lack of linearity in this region indicates poor data quality, and presence of linearity can be an indicator of quality, but linearity itself does not ensure quality.[57, 63] Upturns in this Guinier region demonstrate sample aggregation, whereas downturns in this region shows that the sample may have interparticle repulsion. When modeling data, regions of interparticle effects can be excluded to ensure better fidelity of the models, but it is important to include a graph with the entire scattering profile showing these effects to convey accuracy and integrity when reporting SAXS data.[57, 63]

The next important piece of information that SAXS provides is the called the radius of gyration (*Rg*) which can be estimated via the Guinier approximation using the smallest angle data, where $q*Rg < 1.3$ (Eq. 2).

Eq. 2 $$I(q) \backsimeq I(0) \exp\left(\frac{-q^2 \mathrm{Rg}^2}{3}\right)$$

In equation 2, *I(q)* refers to the intensity of scattering as a function of the scattering vector, *I(0)* is estimated intensity of the scattering at the 0 angle, and q is the scattering vector. This is

calculated from experimental data based on the Guinier approximation from the *I(q)* vs q^2 graph. By rearranging the equation, the *Rg* is found from the slope of the linear fit of these data.[57, 64]

Rg provides a rough estimate of the particle's size, it provides limited structural insight, as it is simply the root mean square distance from each scattering volume to the particle's center of mass. Therefore, the next step in data analysis to go from 1-dimensional data towards an actual model is to perform a Fourier transform on the acquired data to get a pair-distance distribution, also called P(r).[59]

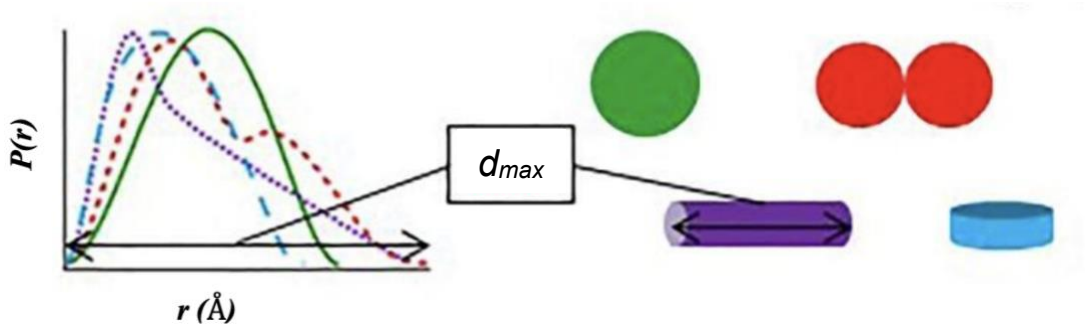

Figure 1.13: This graph shows different probability distribution curves for differently shaped molecules. Reprinted with permission from Oliver *et al* 2019 under the Creative Commons Attribution (CC BY) license (https://creativecommons.org/licenses/by/4.0/).[59]

The P(r) curve is a histogram of distances, indicating which interatomic distances are the most probable in a given particle. The curve always begins at zero, as the probability of finding two atoms inside of one another is zero. At the Dmax, the probability goes to zero as there will not be two atoms further apart that the maximum linear dimension of the particle. This is illustrated with the purple cylinder (**Figure 1.13)**, with the black arrow indicating the Dmax on the curve as well as on the molecule. Overall, the information obtained from the P(r) curve can be used to gain better insights into the global structure.[57, 59]

When analyzing SAXS data, it can be useful to look at examples in the literature of similar molecules. In the below example, the researchers are examining how the SAXS profiles change as i-motifs move from folded to unfolded.

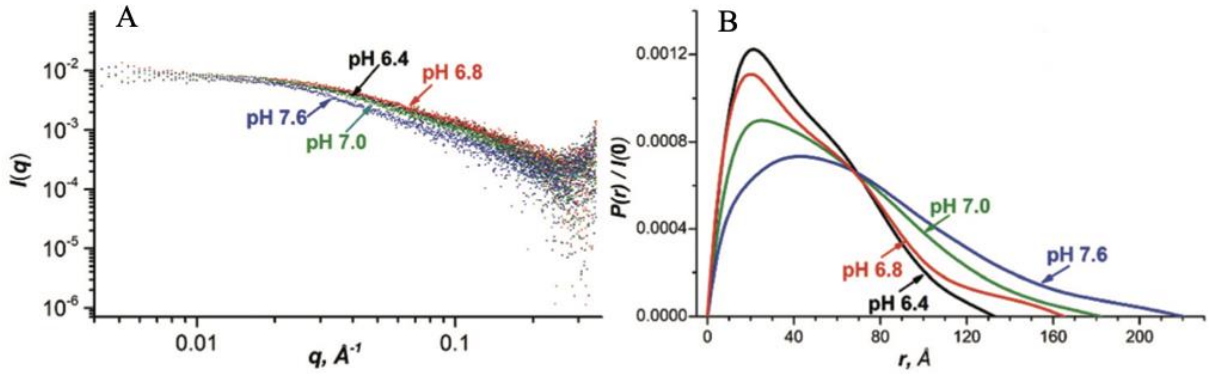

Figure 1.14: (A) Scattering profile of i-motif structure at different pHs and the corresponding P(r) curve (B). Used with permission from Minasyan *et al* 2022; permission conveyed through Copyright Clearance Center, Inc.[45]

Since SAXS is a low-resolution technique, it cannot resolve the specific locations of the bases in the i-motif, but **Figure 1.14** shows that valuable information about changes in structure can be obtained with SAXS. Their sample was 77 nucleotide strand of single stranded DNA that they designed to have shaped like a dumbbell with an i-motif region on either side, connected by a double stranded stem. This paper was a valuable training tool in interpreting SAXS data because it illustrates the structural changes from i-motif in response to changes in pH. Based on prior knowledge of the literature,[7] as the pH increases, the i-motif becomes increasingly destabilized, and loses its distinct structure.[46] Basic structural changes are shown with the q vs I(q) graph where they have different scattering results in response to pH. These changes are more clearly demonstrated in the probability distribution curve in a change in Dmax from 130 at pH of 6.4 to a Dmax of 220 at a pH of 7.6.[45]

Finally, based on the current research on i-motifs in the literature, there is a significant need for standardization of how i-motifs are studied, or at least better acknowledgement of other factors

in experimental design that can lead different conclusions and assumptions. The purpose of this thesis is to study how buffer choice impacts DNA secondary structure by first comparing the circular dichroism spectra of the RAD17 promoter oligonucleotide sequence in tris-borate, tris-acetate and HEPES, second, observing changes in CD spectral peaks in regard to increasing sodium or lithium concentration, and third, obtaining additional structural information on structures present in this oligonucleotide with SAXS. The overall goal is the show that buffer choice can impact which DNA secondary structures are favored, and to determine how buffer identity impacts how readily i-motifs are formed

CHAPTER 2: MATERIAL AND METHODS

2.1 Materials

The single stranded DNA oligonucleotide sequence was purchased from Integrated DNA Technologies (IDT) with the sequence (5'-CCACCCCCCCCCGCCCCCCCCCGGA). Endotoxin free water was used to resuspend the DNA for the stock solution. Trisaminomethane Hydrochloride (tris HCl), ethylenediaminetetraacetic acid (EDTA), ammonium persulfate (APS), urea, and lithium nitrate were purchased from VWR Avantor. For the high throughput (HT) SAXS, clear, full skirt, nonsterile 96 well plates with corresponding sealing mats were purchased from Corning. 0.2 μM centrifuge filters and 3 kilodalton molecular weight cutoff centrifuge filters were purchased from VWR. The Ultra-Low Range DNA Ladder, 100% ethanol for cleaning cuvettes and glass plates, gel loading tips for loading samples into CD cuvettes, were purchased from ThermoFisher. Magnesium chloride and boric acid were purchased from Sigma Aldrich. 29:1 40% acrylamide solution was purchased from bio-rad. The circular dichroism measurements were taken with the Jasco 1500. The SAXS samples were sent overnight with ice packs to the SIBYLS beamline as part of the Lawrence Berkley National Laboratory.

2.2 Buffers

Since Tris-Borate (TB) is very commonly used buffer for nucleic acids, it was the first buffer used.[65] The working concentration of Tris-Borate was 90 mM each with 1 mM of Magnesium Chloride at a pH of 7.4. The TB $MgCl2_2$ buffer was titrated to the correct pH with 6 M HCl. Tris base was used to make the buffers, as this usually requires hydrochloric acid to get it

to a pH of 7.4 due to it starting off too basic. This is preferrable since it won't require the use of a salt hydroxide to adjust its pH.

The next buffer chosen was tris-acetate EDTA to determine if the borate was impacting DNA structure, of if Tris was potentially interacting with the DNA structure. It was also titrated to a pH of 7.4 with 6 M HCl. The Tris Acetate had a concentration of 90 mM and the EDTA had a concentration of 0.5 mM. An important aspect to consider when working with Tris buffers and CD is that below 200 nm, Tris can have a peak, and EDTA is recommended to have a concentration less than or equal to 1 mM.[66] Since the pH of tris is temperature dependent, the temperature of the experiments performed were kept between 20 ^{o}C and 22 ^{o}C. [67]

The third buffer chosen was HEPES because it is structurally significantly different that TB and TAE. The working concentration of HEPES was set at 10 mM per recommendations from the literature[68]. However, since HEPES starts off too acidic, it had to be titrated to a pH of 7.4 with 6 M NaOH which resulted in an overall concentration of 3 mM sodium in the working buffer concentration. There was initial consideration of titrating HEPES with lithium hydroxide, but even 2 mM lithium can destabilize the i-motif structure, as shown experimentally, so sodium hydroxide was used to maintain consistency.

2.3 CD Instrumentation

For the initial experiments, a Jasco 720 was used, and it needed calibration after not being used for around 10 years. The first step is to make a calibration curve. The CD instrument needs to be calibrated every six months with a known standard to ensure it is giving quality results. 1mg/mL of aqueous 0.06% (w/v) camphorsulfonic acid (CSA) in a 1cm cell was used as the

standard. If the instrument is correctly calibrated, the peak value should be 190.4 +/- 1 millidegrees (mdeg). The scale correction knob was used to place the peak in that value.[69]

The next step of readying the CD instrument for data collection is mirror calibration. The mirrors have to be calibrated every six months for optimal performance. Improperly aligned mirrors or mirrors that need to be replaced will cause an increase in HT voltage. This was accomplished by removing the mirror cover on the left side of the back of the instrument. On the sub-panel of the amplifier unit, the "Test Signal" was set to off, the "Indicator selector" Switch: was set to PMV (kV), and the "HT" switch was set to Auto. Small adjustments were then made to the adjustment screws, and the minimum voltage was adjusted so that it was between 200 and 300 volts. Once this was completed, the covers were put back on the mirrors.

After that is the Test Signal Check, and the parameters are shown in **Table 2.1.** This makes sure that the electrical system of the instrument is working correctly. For this test, go to 300 nm. Turn the "Test Signal" knob in the sub-panel of the amplifier unit to "-", "0", and "+", and the should display the following results:

Table 2.1: Parameters for performing the "Test Signal" Check.

Position of "Test Signal" Knob	**Result that should be displayed**
"-"	-18 (+/- 10%) mdeg
"0"	0 +/- 0.1 mdeg
"+"	18 (+/- 10%) mdeg

When finished, turn the "Test Signal" knob back to "Off"

The final maintenance activity performed was the energy check. This should be performed once per year to ensure the instrument is still operating at an optimal energy level. Deterioration of optics will first be noticeable in wavelengths below 250 nm. If the instrument fails the energy check, the mirrors need to be replaced. With this check, the user is observing the HT voltage at 300 nm and at 200 nm with a slit width of 1.0nm. At 300 nm the HT voltage should be between 180 and 250 volts if the sample chamber is empty. At 200 nm, the HT voltage should be 500 volts or below.[69]

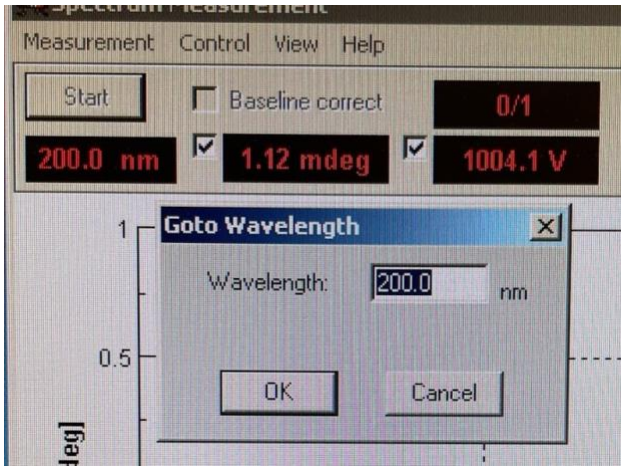

Figure 2.1: Example of a failed energy check.

As seen on **Figure 2.1**, at 200 nm, the HT voltage is 1004.1 V, which is significantly higher than 500 volts. The only way to get the HT voltage to an acceptable range was to increase the slit width to 10 nm, but 5 nm was sufficient for wavelengths above 240 nm. This works because the HT voltage increases in response to inadequate light reaching the detector, so increasing the slit width allows a greater amount of light through. However, increasing the slit width can lower the resolution of the acquired spectra.

Based on the routine maintenance checks, the Jasco 720's mirrors were significantly deteriorated and needed to be replaced. RAD17 was suspended in water for purpose of

convenience and training, and the i-motif was clear in CD spectra. However, there was a significant amount of noise and the resolution was low. In order to obtain quality data, the mirrors will need to be replaced. Based on the hardware manual, they should be replaced every 5 years, and it had been at least 10 years since their last replacement.

Further experiments were conducted using a Jasco 1500 CD instrument. To obtain quality readings, the manufacturer, Jasco suggests a starting range of 10-30 μM of sample. Based on experimental observations, 25 μM worked well to produce quality data with minimal noise, as shown in **Figure 2.2.** The data from the instrument is reported in the units of CD mdeg. In order to more accurately compare data, it must be normalized against concentration and pathlength. This ensures reproducibility among researchers and allows for better interpretation of spectra since different molecular weight species at different concentrations and pathlengths can alter the data generated by CD mdegs.

Eq. 3 $$Molar\ Ellipticity\ [\theta] = \frac{(mdeg)(MW)}{10 * \ell * C}$$

Equation 3 shows the calculations involved from converting CD mdegs to molar ellipticity. MW is the average molecular weight in g/mol, C is the concentration in g/L, ℓ is the pathlength of the cuvette in cm, and θ is the unit for molar ellipticity, and it has the units $cm^2 * dmol^{-1}$.

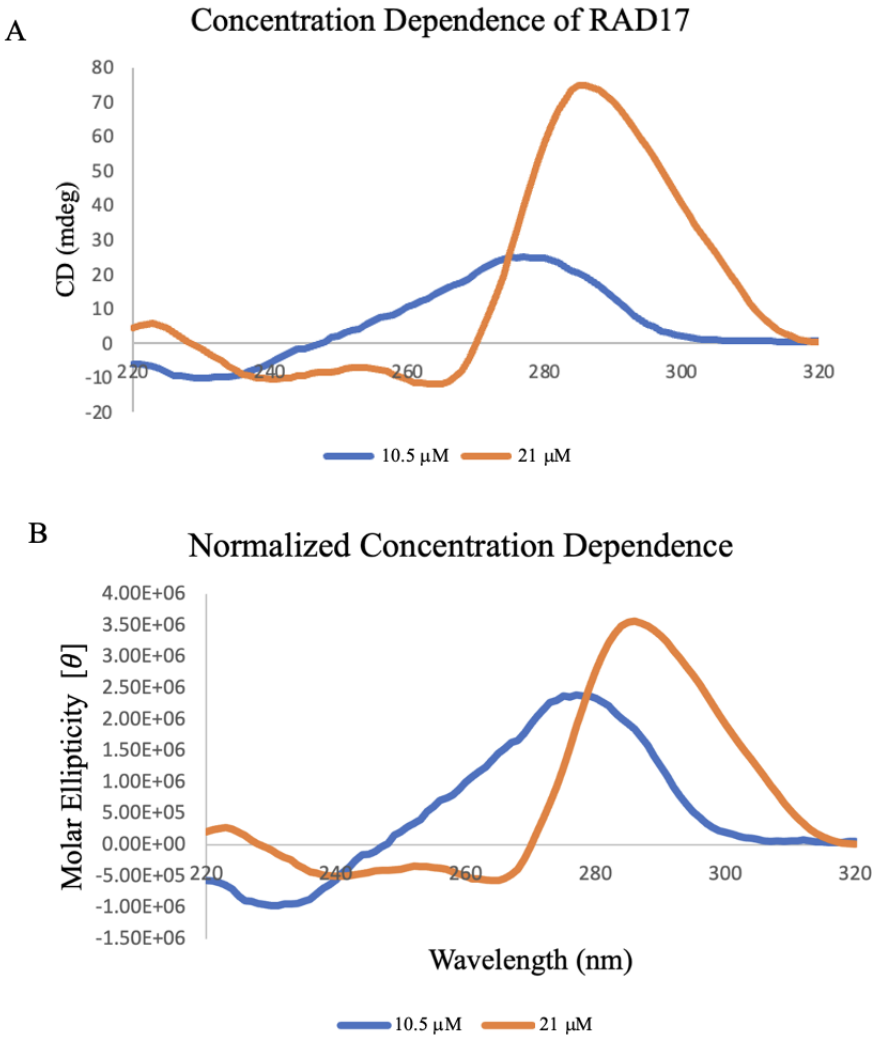

Figure 2.2: CD Spectra to determine appropriate concentration of RAD17. (A) Data directly from the CD instrument reported in CD mdeg. (B) Data that is normalized against concentration and pathlength.

Two different cuvettes were also examined to assess if a 1mm standard quartz CD cuvette or a 0.5 mm de-mountable cuvette worked better (**Figure 2.2)**. The 1mm cuvette has a small neck at the top, which created a slight vacuum, which prevented recovery of about 25% of the sample, and it also made it difficult to clean the cuvette between runs. The 0.5 mm cuvette allowed for no sample recovery, but the advantage for a de-mountable cuvette is that it can be thoroughly cleaned

between samples to reduce the risk of contamination and dilution from cleaning the cuvette between runs.

When comparing CD runs with the two different cuvettes containing the sample and same sample concentration, the de-mountable cuvette showed significant noise whereas the standard 1 mm cuvette did not. Based on these results, it was established that the 1 mm cuvette will be used. The normalized molar ellipticity versus standard instrument output in CD mdeg was also included here to illustrate the importance of normalizing CD data when utilizing a different cuvette or concentration between runs.

CD has minimal sample preparation requirements compared to other techniques, but it does require 95% purity since CD results are based on the species predominately present. A denaturing polyacrylamide gel was used to assess purity (see Appendix), and the results show that the RAD17 is monodisperse and there are no obvious other species present as contamination. The samples were then created to give a final oligonucleotide concentration of around 25 μM, 1X buffer concentration and diluted with double de-ionized water. Once the samples were assembled, they were heated to 95 ºC for 2 min, and then placed on ice.

Before taking a sample measurement, a background measurement was taken at each salt concentration, starting with zero added salt. For HEPES, no added salt includes 3 mM of sodium from titrating the buffer to the created the desired pH of 7.4. The buffer background salt concentration corresponded to the same salt concentration as the sample. In between samples, the cuvettes were rinsed with de-ionized water, and then rinsed three times with the buffer of the sample next to be tested. After the CD runs were concluded, the cuvette was washed with a cell washer with ethanol, rinsed ten times with water and then allowed to dry.

All measurements were obtained on the Jasco 1500 at 22 ºC, a DNA concentration of 25 μM and the parameters utilized are shown in **Table 2.2.**

Table 2.2: Starting measurement parameters for collecting CD data.

Parameter	**Input**
Measure range	320-220 nm
Data pitch	1 nm
Digital integration time: 4 seconds	4 s
Bandwidth 1.00nm	1.00 nm
Scanning speed: 50 nm/min	50 nm/min
Baseline correction:	Yes

These settings described in Table 4 showed appropriate data for the model system used, so they did not need to be adjusted significantly. The measurement range was chosen based on the known peaks of i-motifs and hairpins based on the literature. The buffers chosen also begin to display a signal in the CD spectra right around 200 nm and significant signal below 200 nm. From data collection, the region between 200-220 nm did not provide useful data due to high noise, and i-motifs do not have useful spectral features in this region. The samples containing a higher salt concentration in particular had significant noise, reducing the usefulness of the data collected in this region.

This increase in noise is a result of increasing the HT voltage in response to the less light hitting the detector. Above 700 volts, the data is generally considered to be unreliable. Before running an experiment, the HT voltage should be 200-300 volts. If the HT voltage is higher than that when not taking a CD measurement, the mirrors may need to be aligned. If the HT voltage is

above 700 volts during a run, the sample may be too concentrated or the cuvette may need cleaning. The graphical user interface for CD instrument include a readout of the data in mdegs, but it also displays a graph on the same screen showing the HT voltage as a function of wavelength as a quick quality check while collecting data.[69, 70]

Nitrogen is another key component of CD use. It is very important to purge the system with nitrogen prior to use to avoid damage to the instrument and avoid creating ozone gas, which is a respiratory irritant. Other molecules in the air can also contribute to the reading, obfuscating the signal if the nitrogen purge is not performed. To fully purge the instrument, it is recommended to flow nitrogen for a minimum of 5 minutes prior to using the instrument at 3 to 5 liters per minute, and the recommended flowrate is shown in **Figure 2.3**. Utilizing these guidelines prevent extraneous oxygen from absorbing light that should otherwise by absorbed by the sample.[71]

Table 2.3: Recommended nitrogen flow rate based on wavelength of interest when operating a circular dichroism instrument.

Wavelength	**Nitrogen flow rate**
200nm and above	3-5 L/min
185nm to 200nm	5-15 L/min
180nm to 185nm	15-20 L/min
Below 180nm	>20 L/min

2.4 SAXS Instrumentation

Since SAXS relies on the subtraction of a buffer matched background data set from the experimental data, sample preparation is critical. The presence of impurities or aggregates,

especially the presence of higher molecular weight species can bias the SAXS results to reflect the impurities rather than the desired molecules in the sample. The first method employed to eliminate unwanted products in the solution was polyacrylamide gel (PAGE) purification. This resulted in a recovery of 30-40% of the sample, which is a significant loss.

The two options for SAXS at the SIBYLS beamline are high throughput (HT) and size exclusion chromatography (SEC) SAXS. HT-SAXS requires a 96 well plate to be sent to expediate sampling. Each well should contain 30 μL of combined buffer with the sample. To minimize concentration dependent effects, they recommend for each sample, having 3 different concentrations, with the concentrations ranging from 1 to 10 mg/mL. However, this guidance appears to be for proteins, which have a lower electron density than nucleic acids, leading to a weaker scattering. Due to nucleic acids having approximately double the scattering length density as proteins, the initial concentrations used for SAXS were 40, 20, and 10 μM.

For the first iteration of SAXS, HT SAXS was utilized to quickly assess structural characteristics of the various metal ion titrations of RAD17. SEC-SAXS is limited to 7 samples, and since the DNA was purified by gel, HT SAXS was considered to be a reasonable first step. The samples were prepared with a final RAD17 concentration of 40 μM in 1X Tris-Borate Magnesium 7.4 buffer in a volume of 60 μL. Although Tris-Borate collapses the i-motif structure, the SAXS experiments were performed in a parallel approach due to difficulties in scheduling CD time, and due to beamtime limitation with SAXS. Knowing that Rad17 in TB does not form i-motifs, it will be a useful comparison to future SAXS experiments that are conducted with HEPES. The samples were created as described in **Table 2.4:**

Table 2.4: Salt concentration contained in samples sent for HT SAXS.

Ion concentration	Significance
No lithium or sodium	Negative control
1 mM Lithium Nitrate	Therapeutic level of lithium[41]
4 mM Lithium Nitrate	Severely toxic blood concentration of lithium[41]
8 mM Lithium Nitrate	2X severely toxic lithium concentration
40 mM Lithium Nitrate	10X severely toxic lithium concentration
50 mM Sodium Nitrate	Below most accepted sodium concentration (100mM) that de-stabilizes i-motifs. [7]
150 mM Sodium Nitrate	Above most commonly accepted de-stabilization value.[7]

Once the samples of various lithium and sodium concentrations were made, the samples went through dialysis to assist with buffer matching. The dialysis had a molecular weight cutoff of 3.5 kDa, which was the ideal size to retain the oligo in the dialysis cup given that the RAD17 promoter oligo fragment used is around 7.3 kDa. The samples were dialyzed against their matching salt-buffer dialysate overnight, and then the dialysate was switched out for fresh buffer-salt solution and dialyzed again for two hours. This process was repeated 3 times, with the final dialysate being used as the buffer match for SAXS analysis.

Once dialysis was complete, the samples and separately their matched buffers were filtered with 0.2 μm centrifuge filters at 12,000 RCF for 5 min. The concentration of each sample was then checked with a Nanodrop spectrophotometer.

A non-denaturing gel was run to confirm that DNA was free of significant aggregates and to confirm the presence of DNA in each sample. The far-left band illustrates the ladder, which was mixed 1μL ladder, 1 μL native loading buffer, and 4 μL of endotoxin free water. Wells 2 through 8 show the various samples mixed 2 μL sample with 2 μL of native loading buffer, with 2 μL loaded in each well. The results are shown below:

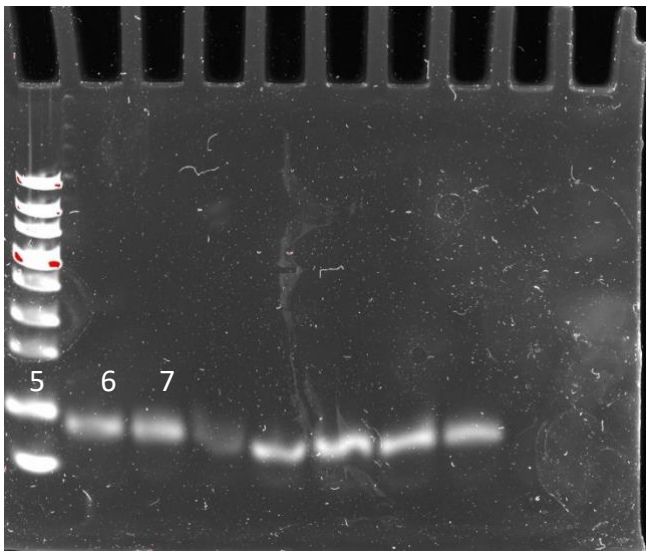

Figure 2.3: Native gel of RAD17 after dialysis and filtration. The numbers correspond to the sample numbers listed above starting with 0 sodium or lithium (1), increasing lithium concentration (2 to 5), and then increasing sodium concentration (6 and 7). The ladder used is the same ladder as above, with the top band being 300 nucleotides, and the bottom band is 10 nucleotides.

As shown in **Figure 2.3**, all 7 of the samples contained DNA and appear to be monodisperse. The bands are not as consistent as desired, but this could be due to poor loading, or it could be due to partial denaturation during the electrophoresis experiment. The running buffer was chilled in 4^{o}C prior to running, and the entire apparatus was run at 4 °C. However, the running buffer after the gel was finished was significantly warm, which could account for the bands not being straight if denaturing started to occur. Despite these issues, the gel did appear to be free of

any aggregates, and all the prepared samples did include DNA, indicating these sample would likely be acceptable for HT-SAXS experiments.

The samples were sent as a concentration series with each sample having the full concentration present post-dialysis and filtration, one at 50% concentration and the other at 25% concentration. In setting up the SAXS experiments the beamline permits the user to specify when they would like the sample cell washed to help reduce contamination between samples. Per their recommendations, the buffer match was placed in the cell proceeding and immediately after a concentration series. Having a buffer match in two different wells increases the likelihood of a quality buffer subtraction in the even there is error when collecting one of the buffer only samples. After each concentration series at a given salt concentration, the cell was washed, and the next well collected would be the buffer match of the upcoming concentration series.

For size exclusion chromatography (SEC) SAXS, the SIBYLS beamline allows 7 samples with one buffer. Due to the differences in samples being the different buffer conditions, this limits the number of unique samples to only one per beamtime for the purposes of this research. Based on initial CD data, RAD17 in HEPES at 3 mM sodium forms i-motifs, so that is the sample that was sent for the second iteration of SAXS. SEC also requires a higher concentration as well as volume, so 300, 150, and 75 μM DNA were used in the sample wells, with a final sample volume of 60 μL.

RESULTS AND DISCUSSION

3.1 Structural prediction with NUPACK software

NUPACK (Nucleic Acid Package) is a software that utilizes nucleic acid sequences to generate the most probable structure based on free energy calculations. One limitation, however, when studying DNA secondary structures w with NUPACK is that it is programmed to only predict Watson-Crick base pairing.

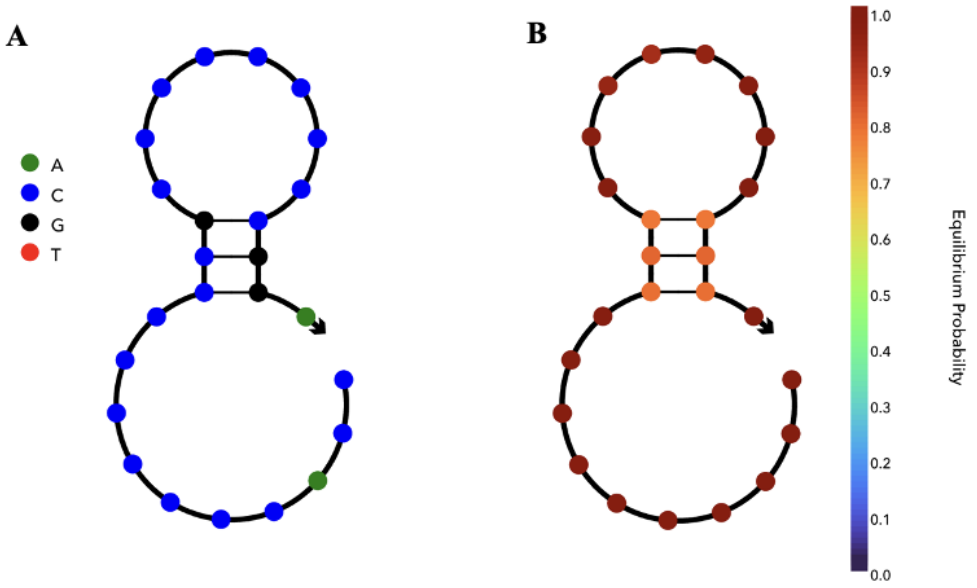

Figure 3.1: NUPACK structural prediction based on portion of RAD17 promotor sequence input. A shows the structure in terms of nucleotide bases represented by blue dots (cytosine), black dots (guanine), and green dots (adenine). B is showing the probability of this structure existing at equilibrium with the darkest red showing the highest probability, and the orange showing a slightly lower, but still reasonably high probability. [72, 73]

Based on the NUPACK predictive model, a potential structure that the RAD17 promoter oligonucleotide sequence could adopt is a short hairpin and a long single stranded region. While the software is not designed to predict i-motifs, this model has value in that it is a different potential structure that this sequence could adopt. **Figure 3.1A** shows NUPACK utilizing canonical base pairing with the only pairing interactions between cytosines and the three guanines present.

Additionally based on the software algorithm, this structure has a very high equilibrium probability, as seen by the dark red dots in **Figure 3.1B**.[72]

3.2: Comparing buffers with CD

The first buffer examined was Tris-Borate Magnesium Chloride because it is commonly used in nucleic acid studies.[36] However, unlike what the literature suggested,[46] the structure favored in this buffer system was a hairpin. Lithium was then added to the system to elucidate potential structural changes that may deviate from the hairpin. As seen in **Figure 3.2**, the structure is consistently a hairpin. Concentrations above 8 mM lithium are not biologically relevant, so this concentration was chosen as the highest one tested.[41]

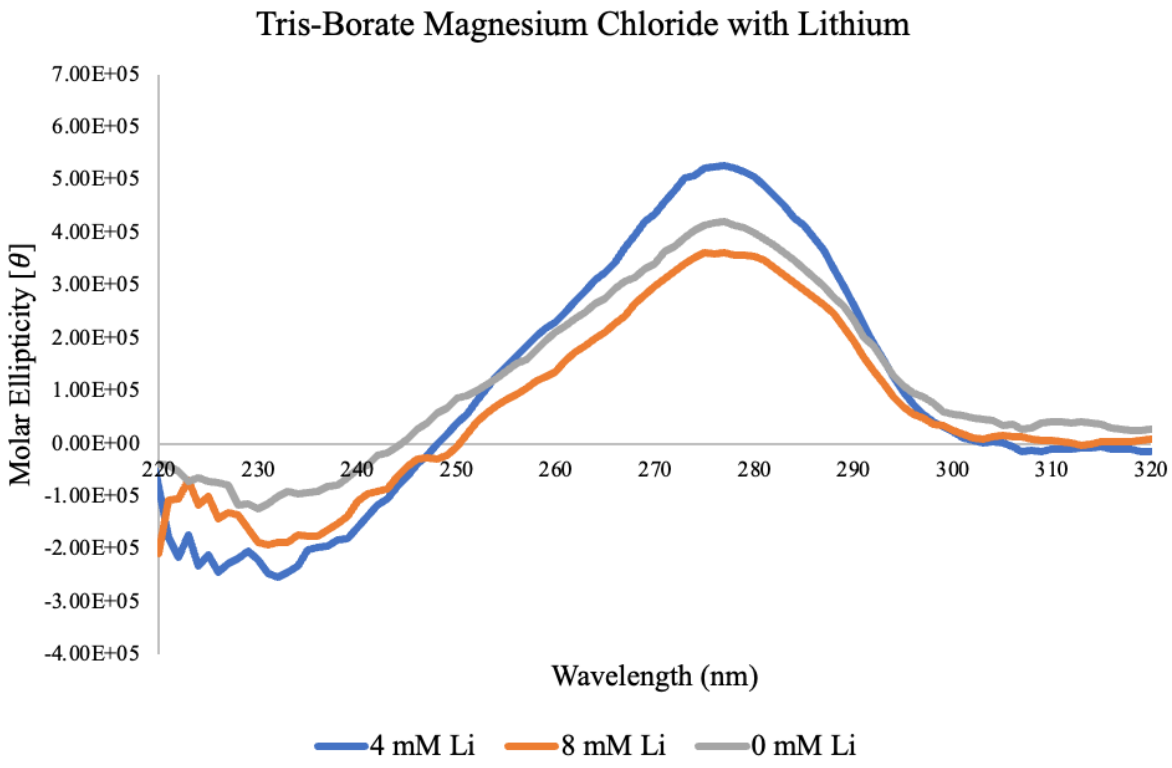

Figure 3.2: Lithium titration series of 25 μM RAD17 in TBMgCl$_2$ pH7.4 and 22 °C

After the first set of experiments with Tris-Borate and RAD17 showed no i-motif formation, more background research was conducted in the literature to ascertain a possible reason for Tris-Borate to collapse the i-motif in a sequence known to readily form i-motifs. There were very few papers looking into how buffers may be interacting with DNA, but one of the proposed mechanisms suggested that the borate was complexing with the phosphate backbone of DNA.[74] As such, tris-acetate was also tested (**Figure 3.2**), but tris-acetate also favored hairpin structure instead of i-motifs. The consistency of results in tris containing buffers favoring hairpins leads to the conclusion that tris may be favoring hairpin formation as evidenced by the broad, positive peak around 280 nm, and lack of a clear negative peak around 265 nm.

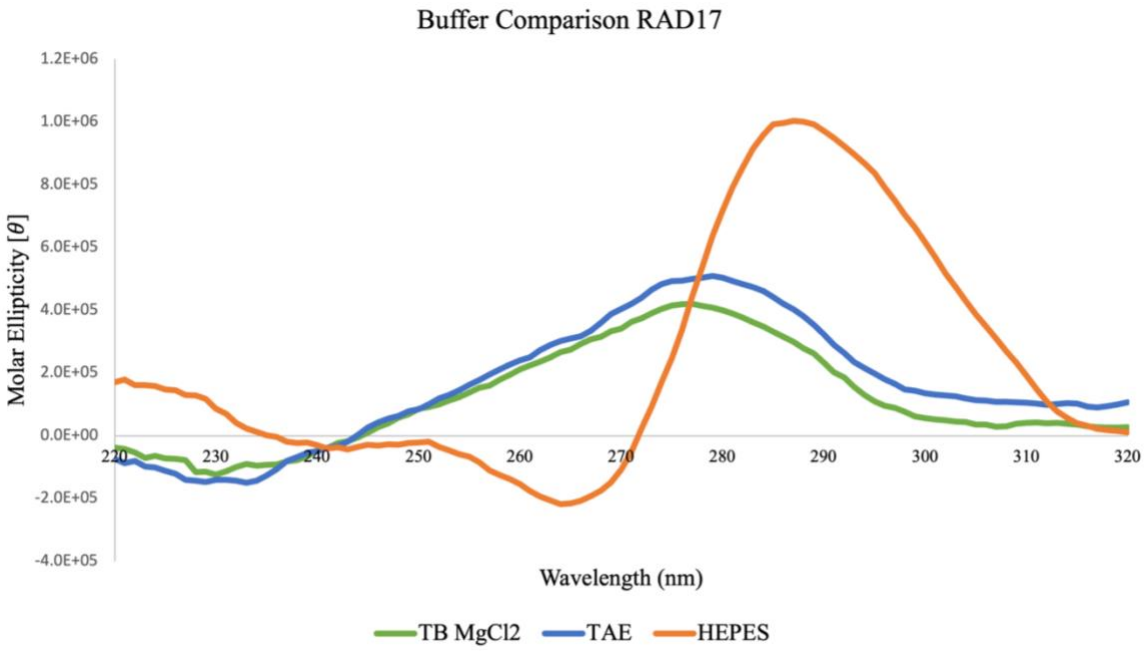

Figure 3.3: Circular Dichroism spectra of HEPES, TAE, and TB with 25 μM RAD17, pH 7.4, and 22 °C.

It is likely the Tris is opting for a hairpin structure as opposed to an i-motif regardless of if it is Tris Borate or Tris Acetate (**Figure 3.3**). Since HEPES is more conducive to forming the i-motif structure, HEPES was used moving forward as the buffer of choice. **Figure 3.3** shows that buffer choice is critical when conducting DNA structural studies.

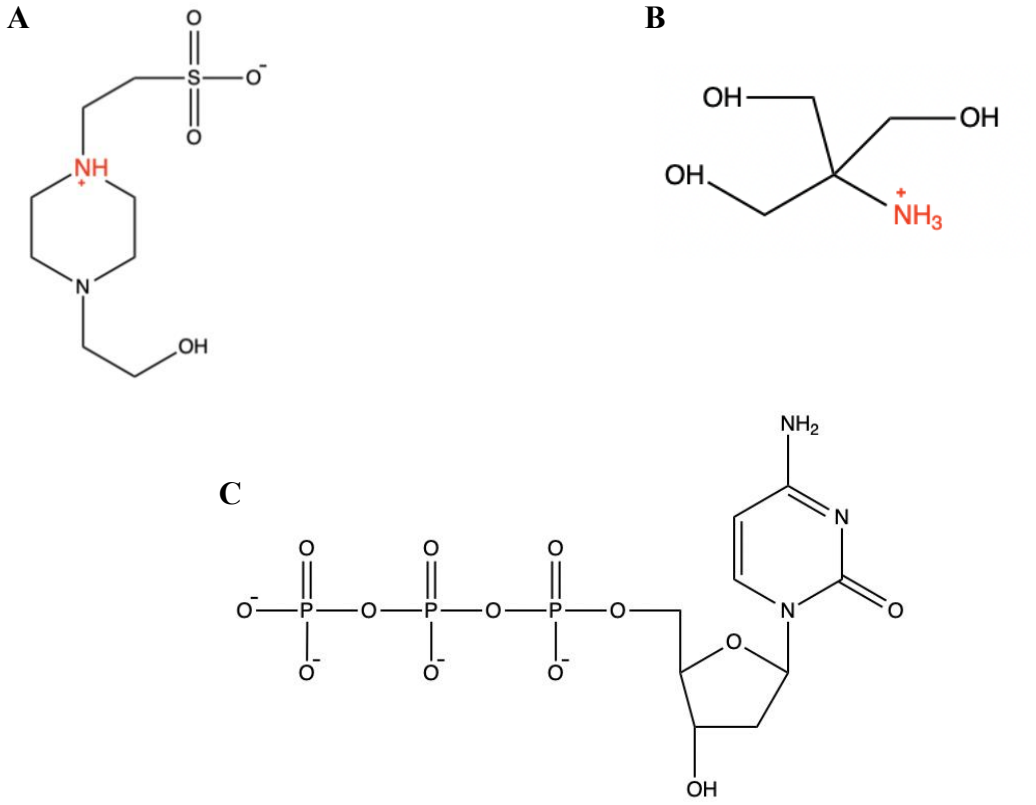

Figure 3.4: Illustration of the structure including protonation states of (A) HEPES, (B) tris, and (C) cytosine at pH 7.4. Protonated sites are shown in red. Image created with ChemDraw.

One recently presented theory is that the phosphate backbone of DNA can act as a weak Lewis base, and the buffer could act as a weak Lewis acid.[74] This could be a logical explanation given that at the physiological pH of 7.4, the phosphates in DNA are negatively charged, and a proportion of the amines in the buffers can be protonated. A popular term for this type of interaction is referred to as "buffers as ligands".[75, 76] A hypothesis as to why this interaction would favor

hairpins is because of the structural differences between tris and HEPES. Tris has a primary amine which makes it more available to associate with the phosphate backbone. The amine on HEPES is tertiary, which sterically makes interactions with the backbone more difficult, but HEPES also exists as a zwitterion at a pH of 7.4. This also is not conducive to interacting with the backbone because it places the negatively charged oxygen closer to the negatively charged backbone, which is not electrostatically favorable.

Another potential explanation as to why tris may be more likely complexing with the phosphate backbone is that the pKa of tris[77] is 8.3, and the pka of HEPES[78] is 7.55. Using the Henderson-Hasselbach Equation, at a pH of 7.4, 89% of the tris species will be protonated compared to 59% of the HEPES species will be protonated. If there are a greater amount of protonated species present with tris, it would be more likely interact with the phosphate backbone via electrostatic interactions and hydrogen bonding.

Based on these structural assumptions, if tris is potentially complexing with the phosphate backbone, this could explain why tris favors hairpins while HEPES favors i-motifs. The association of the tris groups with phosphate would inhibit folding into an i-motif because of potential steric hindrance between the bound tris and the phosphate backbone. To further verify this hypothesis, the pH of the oligonucleotide solution could be increased so that there are less protonated buffer species present. If a higher pH leads to i-motif formation in tris, this would help verify the hypothesis of the mechanism of tris buffers interacting with DNA. The issue with this approach is that increasing the pH of the oligonucleotide solution would likely require other factors to stabilize the i-motif, such as with polyethylene glycol, which does introduce additional variables. Another study that would aid in validating this hypothesis would be to test if other buffers containing primary amines also facilitated hairpin formation. Very few buffers with

primary amines are recommended due to their reactivity, but glycine would be one option. The issue with glycine is that its buffering region is reported to be 2.2 to 3.6,[79] so to test protonation effects, the pH of the oligonucleotide solution would be very far from the physiological pH of 7.4. I-motifs are not stable at very low pH values, so that could influence results.[17] Furthermore, since the techniques used here are low resolution, this hypothesis would need to be validated with a method that can provide detailed information about atomic locations such as NMR.

3.3: CD studies titrating lithium and sodium in HEPES

Once HEPES was found to be the buffer that favored forming i-motifs, the differences in i-motif structure in response to increasing salt concentrations were investigated for sodium and lithium. For the lithium series, there was no difference in CD spectra between 0 and 1 mM lithium, but a significant change was observed at 2 mM. Lithium as a therapeutic agent has a very narrow therapeutic range, with 0.8-1.2 mM as the ideal plasma concentration.[80] Even increasing the concentration in the plasma to 1.5 mM can lead to side effects such as nausea or vomiting, with 3.5 mM or higher being considered severely toxic and potentially lethal with symptoms such as seizure and coma.[41] There is extensive research from the literature from the past several decades, but there is no clear mechanism of action that details how exactly lithium works as a drug, nor is there a mechanism as to how it exerts its toxic effects.[40] Most of what is explained in the literature is a series of corollary effects observed in patients while taking lithium, but nothing definitive has been found.[40, 80] A potential interaction between lithium as a pharmacological agent and i-motifs has been posited by a couple of papers, but it is not something that has been explored in depth.

Showing this clear DNA structural change when going from a therapeutic to a toxic dose of lithium could demonstrate the beginning of a potential mechanism as to how lithium is exerting

toxic effects, but much more research is needed to validate and support such an assumption. It would also be worth investigating how DNA structure changes in response to lithium levels in gene regions that are implicated in mental illness to explore the therapeutic mechanism as well.

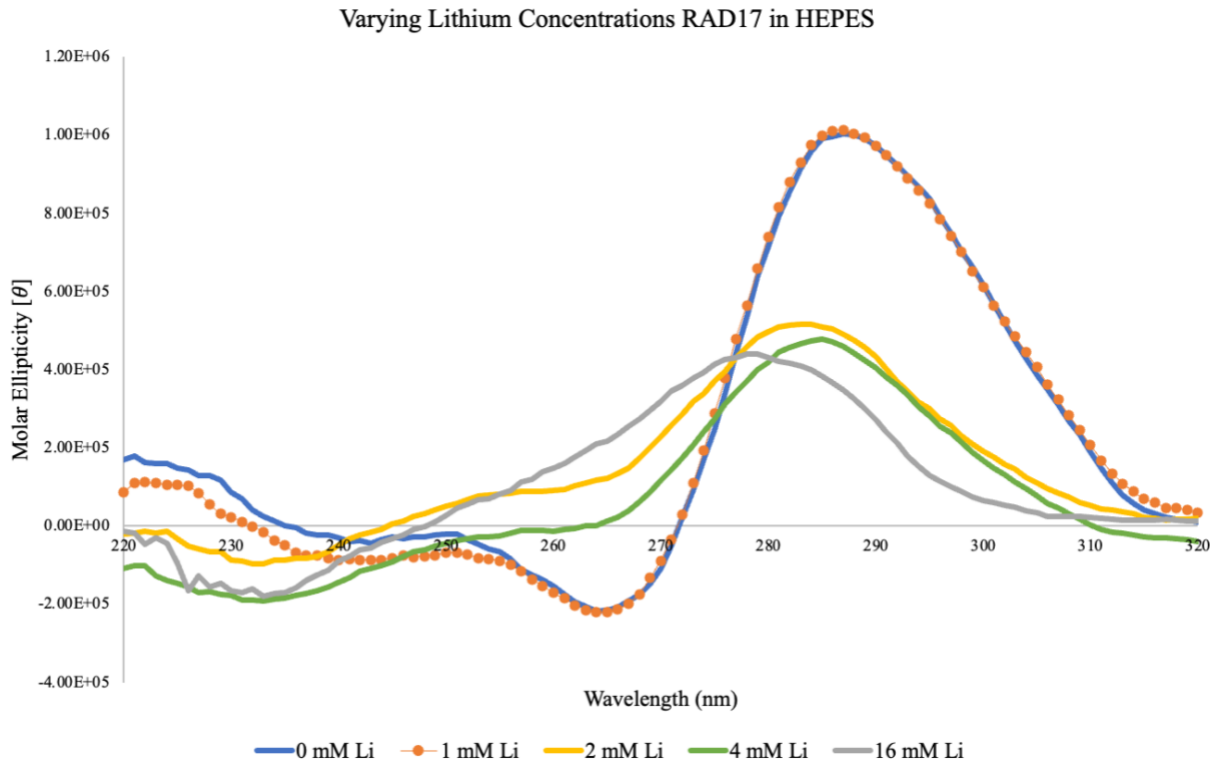

Figure 3.5: CD spectra of increasing concentrations of lithium with 25 µM RAD17 at pH 7.4 and 22 °C. Markers are included on the 0 Lithium line to visually illustrate that the 0 Lithium curve is present but looks very similar to 1mM lithium curve that is overlayed on top of it.

Based on the data illustrated in **Figure 3.5**, RAD17 adopts an i-motif structure in HEPES at 0 lithium and at 1mM lithium, but switches to a hairpin structure between 1 and 2 mM. At concentrations higher than 2 mM lithium, additional structural changes were observed, but not as significant as the 1 to 2 mM transition.

The next cation examined in this research is sodium. Sodium is a much more common cation to study and occurs more naturally *in vivo* than lithium. There is also has very little

agreement among the scientific community as to what sodium concentration de-stabilizes i-motifs. Most sources agree that 100 mM sodium is the point at which the i-motif structure collapses, but this is still contentious as well.[7, 24, 28]

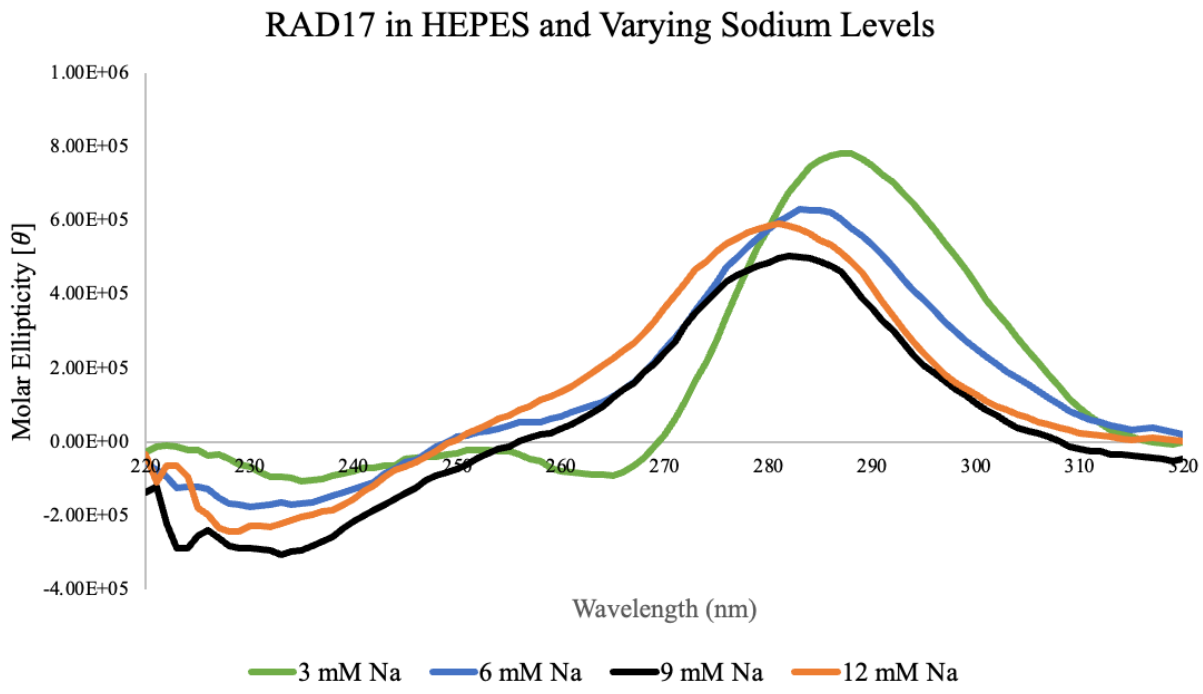

Figure 3.6: Sodium effects on DNA secondary structure at near intracellular concentrations with RAD17.

Based on the results above in **Figure 3.6**, 3 mM sodium shows the sharpest i-motif peak, which is the lowest concentration of sodium that could be obtained after adjusting HEPES to the correct pH without the introduction of other cations to the system. The original plan had been to titrate HEPES with lithium hydroxide instead of sodium hydroxide so there could be a data point with actually 0 mM sodium. However, since earlier results show that values of as little as 2 mM lithium de-stabilize the i-motif, it is likely that the final concentration of lithium in the buffer to obtain a pH of 7.4 would be greater than 2 mM. There was consideration of using a different hydroxide containing compound, but ultimately sodium hydroxide was still utilized to pH the

buffer to maintain consistency between experiments. This is why the concentration of sodium in the titration series starts at 3 mM, and the subsequent concentrations are taking the 3 mM of sodium present in the buffer into the final concentration listed. Furthermore, sodium is also found inside cells at a concentration around 10-15 mM, so a sample without sodium at all is likely to have minimal biological relevance.[38, 81]

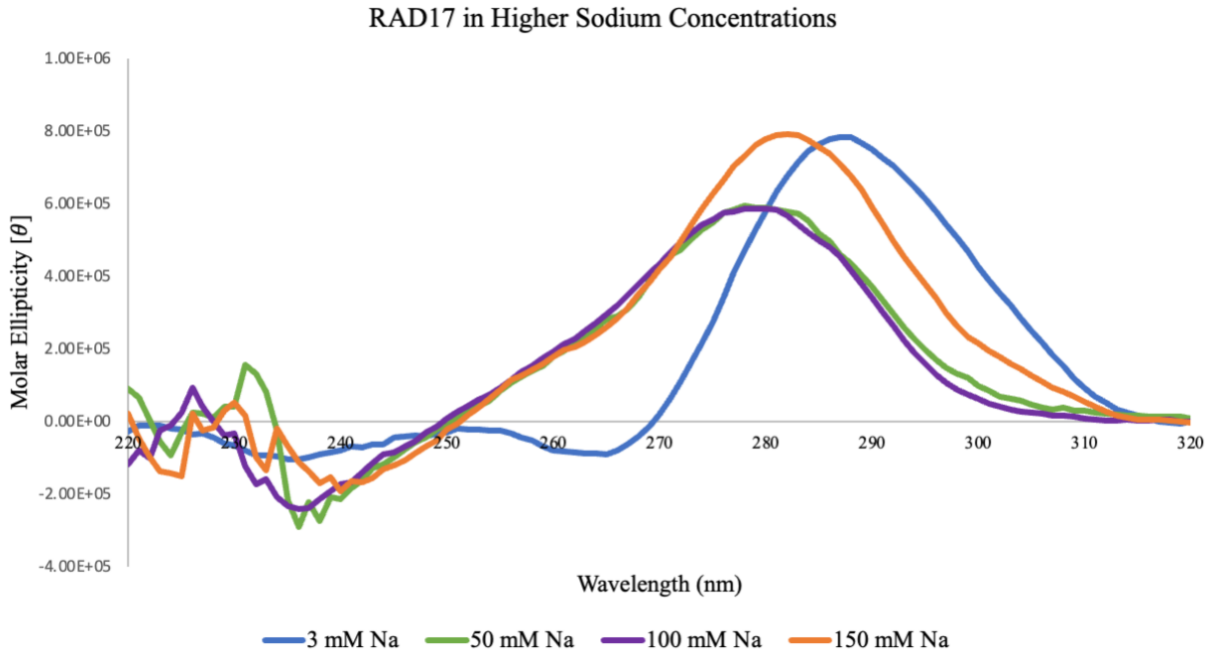

Figure 3.7: Observing CD spectral shifts with increasing concentrations of sodium with RAD17 in HEPES buffer.

In **Figure 3.7**, even though the amplitude of the peaks are changing with increasing sodium concentrations, the most notable spectral change is a shift to the left. In the literature, 100 mM sodium is the most commonly agreed upon concentration that causes de-stabilization of the i-motif.[7] The 50 and 100 mM sodium curves are more indicative of hairpins as opposed to i-motifs. It is interesting to note that 50 and 100 mM sodium have similar curves, but 150 mM sodium indicates another potential structural change. CD spectra de-convolution software be useful in ascertaining more information from this data.

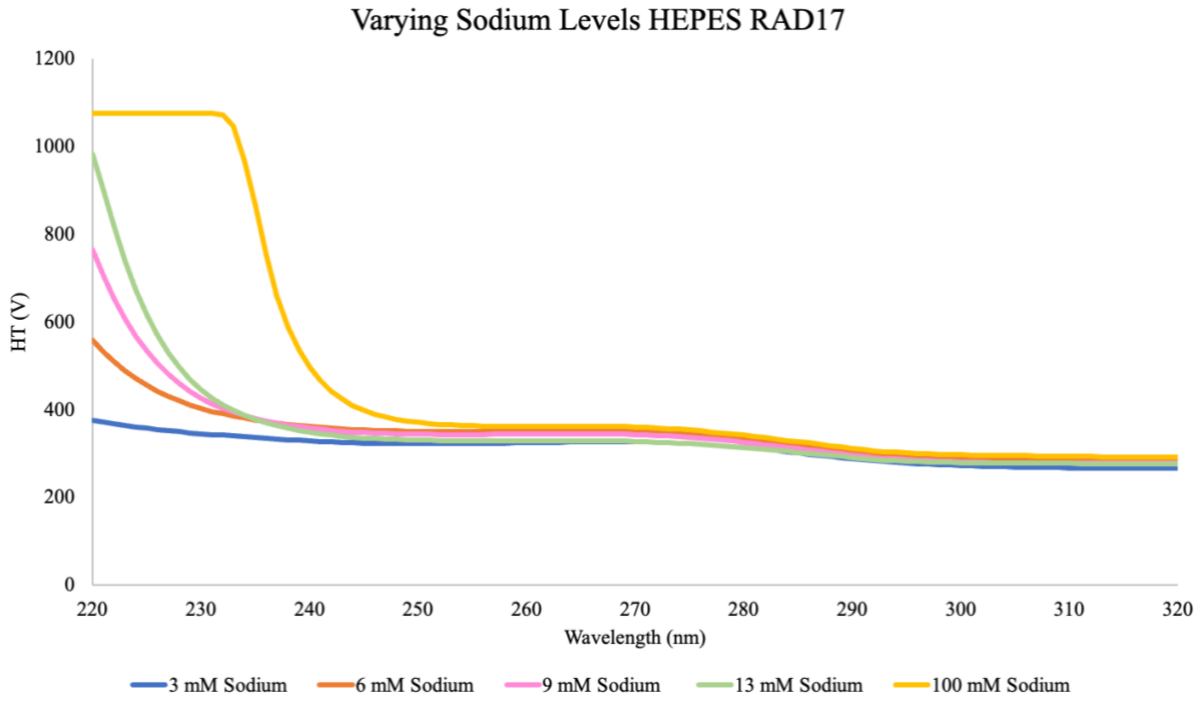

Figure 3.8: HT voltage spectra of RAD17 in HEPES pH 7.4.

When examining CD spectral data, it is important to also consider the HT voltage graph. It is generally accepted that reported CD data has taken the HT voltage into consideration, but this HT voltage graph is included here because of the significance of the noise below 250 nm. As can be seen in **Figure 3.7,** below 250 nm the curve looks jagged and noisy. The reason for that is shown in **Figure 3.8**, that below 250 nm, the HT voltage increases substantially, especially as the sodium concentration increases. Salt has been known to increase absorbance in CD, leading to an increase in noise, so this data is consistent with the literature.[70, 82] HT voltage values above 700 V indicate unreliable data, which indicates that the CD signal below 250 nm cannot be used to draw conclusions from. Since the main wavelengths for i-motifs are at 265 and 288 nm, this is not a significant issue, but it does limit additional interpretation in the low wavelength regions.

For the sodium titration series, the structural changes from i-motifs were more gradual and may suggest an i-motif/hairpin hybrid species. There were not significant structural changes though when compared to the drastic structural changes of the lithium studies. One explanation for this difference could be the size difference between the two cations. NMR data from the literature found that the distance between cytosines in an i-motif structure is about 1.8 Å. [21] The ionic radius of lithium is reported to be 0.7 Å, whereas the atomic radius of sodium is greater than 1 Å.[21, 83] The size of lithium allows the ion to fit in the intercalation distance, which could de-stabilize the i-motif structure, but the sodium ion with a larger radius, may not be able to intercalate as easily.[83] Even though the hydrated ionic radius of sodium and lithium are 2.3 Å and 2.5 Å, respectively[84, 85], de-solvation is required for ion-DNA binding.[86]

The results found here that lithium is Inducing an apparent structural change whereas sodium structural changes are less obvious and less pronounced is supported by the literature.[21] If lithium is able to replace the hydrogen atom intercalated between the cytosines, it would not be able to replicate the same oscillating double-well potential characteristic that occurs in the hydrogen that is typically found on the N3 nitrogen of i-motif cytosines.[21] This could be leading to the disruption of i-motif structure shown in the CD spectra, while sodium with its larger size, may not be able to intercalate between the cytosines, which could explain why its structural changes were less clear. However, more studies are needed to confirm this hypothesis.

3.4: SAXS Data

The first SAXS experiment performed was HT SAXS with the SIBLYS beamline because it allowed testing of many different samples with different buffer compositions. Since quality buffer match is critical for appropriate buffer subtraction, any changes in ion concentration must

be reflected in the buffer for an appropriate match. The samples sent were the RAD17 promoter sequence oligonucleotide fragment in Tris-Borate Magnesium Chloride at pH 7.4.

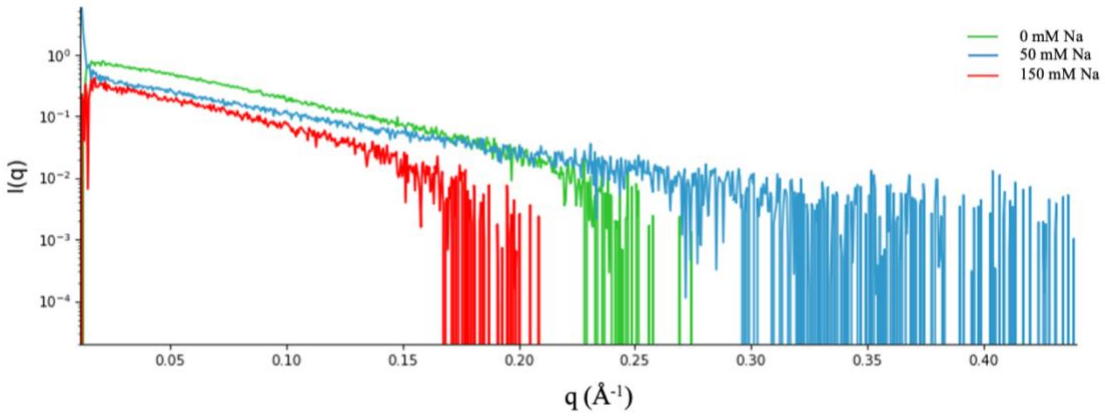

Figure 3.9: SAXS data collected for the sodium series for no sodium (light green), 50 mM Na (blue), and 150 mM Na (red) for the RAD17 oligonucleotide sequence in tris-borate magnesium chloride pH 7.4. The graph was generated with the BioRaw software.[87]

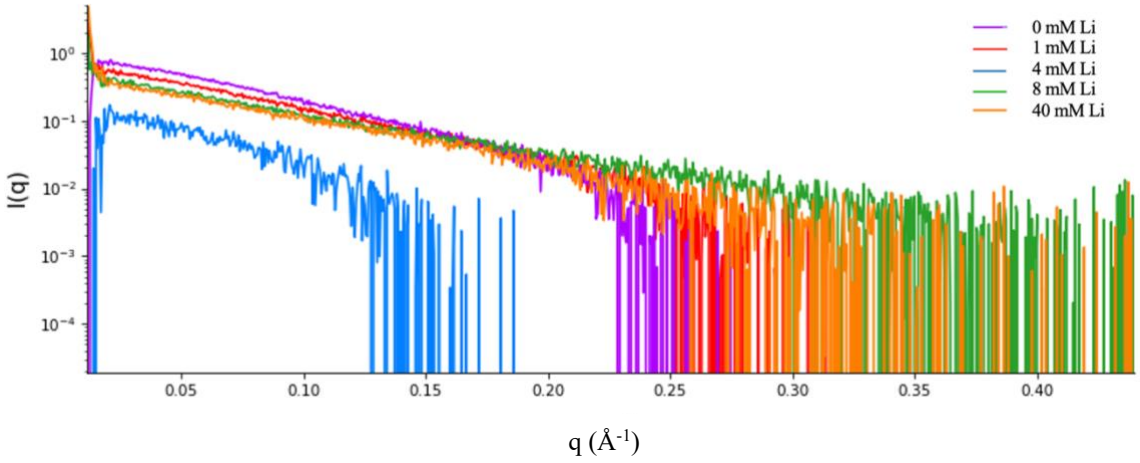

Figure 3.10: Scattering profile of the RAD17 promoter sequence with the lithium series with 0 mM lithium (purple), 1 mM Li (red), 4 mM Li (blue), 8 mM Li (green), and 40 mM Li (orange). for the RAD17 oligonucleotide sequence in tris-borate magnesium chloride pH 7.4The graph was generated with the BioRaw software.[87].

The first step in SAXS analysis is to examine the scattering profiles. Based on the difference in the scattering curves of the lithium experiments in **Figure 3.10** and sodium experiments in **Figure 3.9**, there are likely structural changes induced by different amounts of sodium and lithium. However, due to low concentration and potential aggregation, the sample assumptions from the data are limited. The highest concentration of DNA was 40 μM, and while two lower concentrations of DNA were also submitted, but they did not have a strong enough scattering signal to allow for adequate buffer subtraction. Of the data obtained, the 40 μM DNA with 1 mM lithium sample had the clearest data and is shown in red in **Figure 3.7.** This sample is what was utilized going forward with the analysis.

After looking at the scattering profiles, the next step was to perform a linear fit of the Guinier region. This can quickly tell the researcher if there are quality concerns with the data. However, the inverse is not necessarily true. Observing linearity in the Guinier region can be indicative of quality data, but additional data analysis is warranted to validate claims about data quality.[63] When using a software suite such as ATSAS, the Guinier region is often accompanied by a residual plot, which helps the user evaluate goodness of fit of the data to the line. The data points in the residual plot should appear to be centered around the x axis, and they should look to be randomly distributed. Any systematic deviation from the line of best fit indicates interparticle effects such as aggregation or repulsion.[57]

In analyzing the 1 mM lithium in tris-borate sample, the upward trend of the low-angle region intensities in **Figure 3.11A** is likely indicative of interparticle attraction or aggregation. These interparticle effects can be minimized by utilizing size exclusion chromatography coupled to SAXS by separating the higher molecular weight aggregates from the monomer species.[88] Despite clear interparticle effects in the very low q region, a fit of the linear range provided an Rg

of 22.3 ± 0.4 Å (**Figure 3.11A**), and the residual plot showed a reasonable fit of the data to the line, but there is a slight curve, further illustrating slight particle attraction (**Figure 3.11 B**).

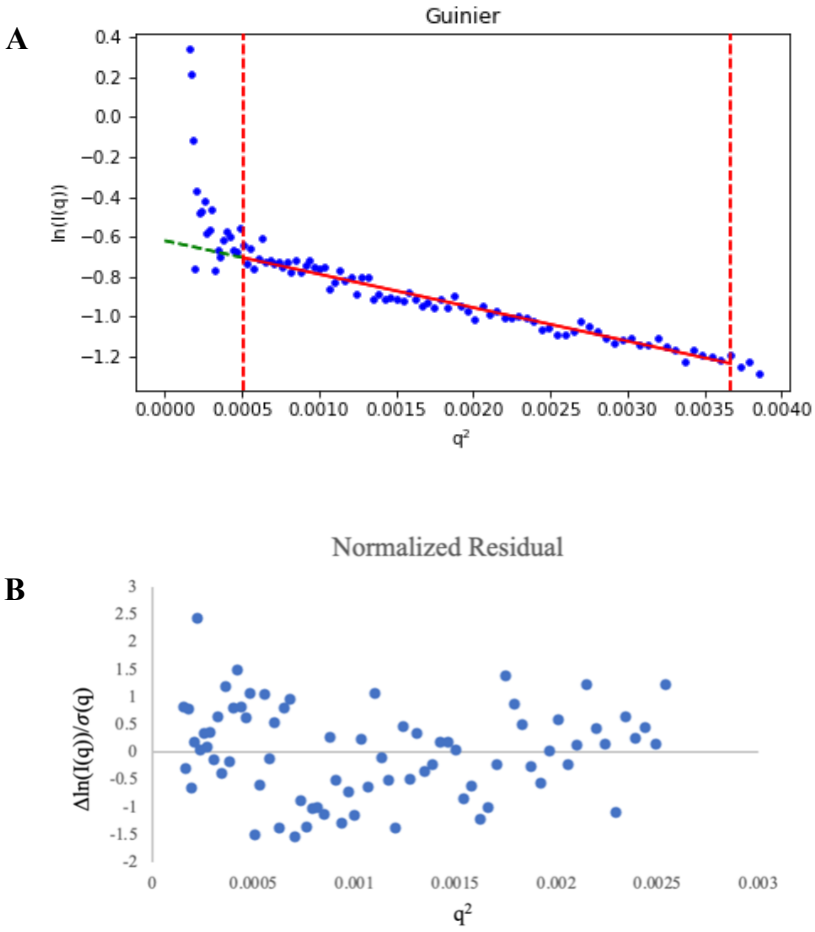

Figure 3.11: 1mM added lithium. (**A**) is the linear fit in the Guinier region, but the data before the Guinier region illustrates interparticle aggregation. The Rg from this data set was 22.29 +/- 0.40 Å. (**B**) is the residual plot. Data was plotted with Primus from the ATSAS sofware.[6]

Next, the probability distribution curve was generated with the GNOM program as part of the ATSAS software suite. This software performs an inverse Fourier transform on the 1-dimensional scattering data to create a probability distribution curve that tranforms the data from reciprocal space to real space. This curve is also called P(r), and it shows the likelihood of certain interparticle distances to assist with determing global structural characteristics such as domain organization, maximum linear dimension, and the *Rg*.[89]

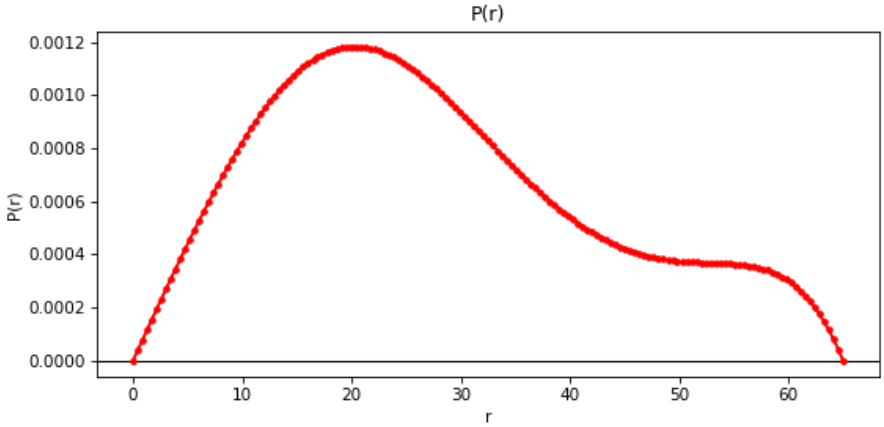

Figure 3.12: P(r) graph of 1 mM added lithium RAD17 from SAXS data. The Dmax is shown to be around 65 Å. The units for the P(r) on the y axis are arbitrary units. Data was plotted with the ATSAS and BioXTAS RAW software.[4]

The *Rg*, as determined by the P(r), is 22.0 Å ± 0.5 Å, which is within the calculated error of the *Rg* from the Guinier approximation. *Rg* consistency between these two methods indicates the aggregation issues noticed in the low q region may be minimal, and the data is useable. Further experiments with SEC SAXS are still warranted, though, to validate these results.

Furthermore, in **Figure 3.12** the peak at 20 Å corresponds to the width of double stranded DNA[90], and the right sided x intercept is referred to as the Dmax, or the longest distance in the molecule[57], which in this case in 62 Å. This is a reasonable Dmax because the distance between nucleotides in DNA is about 0.34 nm,[90] so for a 25-nucleotide sequence, the maximum distance possible, assuming a completely linear structure would be 85 Å. Based on the NUPACK structural predication described earlier, a structure with a maximum length around 65 Å and a width of 20 Å would indicate partial folding, such as with a short hairpin region and a longer single stranded region. Hairpins can exhibit a width of 20 Å like double stranded DNA. If the oligonucleotide was completely folded into a hairpin, the maximum length would be expected to be closer to around 43 Å. These structural assumptions are supported by the CD data as well that a hairpin is the

predominate secondary structure present in the RAD17 promoter oligonucleotide sequence in tris-borate.

In an attempt to address the possible low scattering and aggregation issues seen in the HT-SAXS data, SEC-SAXS was used with higher concentrations of 300, 150, and 75 µM.

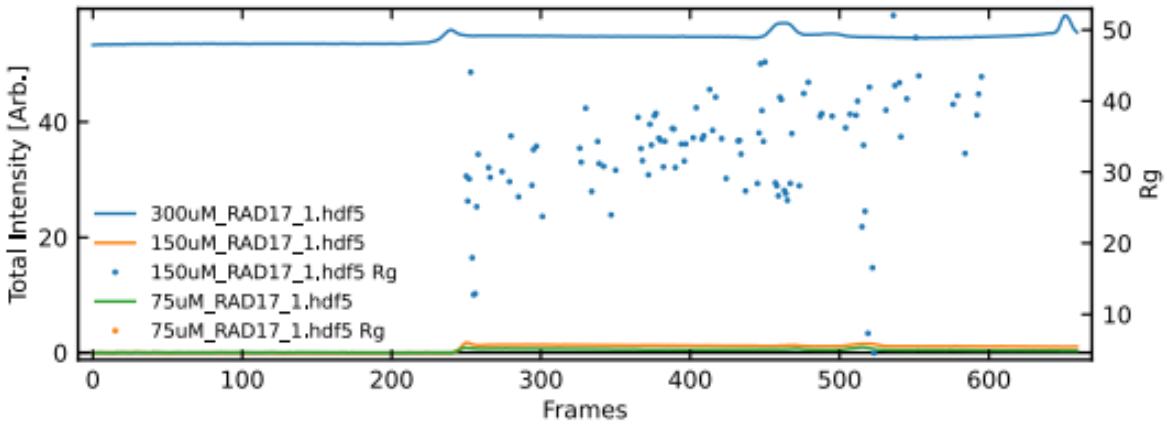

Figure 3.13: SEC SAXS chromatogram for the 300 uM sample (blue line), 150 µM sample (orange line), and the 75 µM sample (green line). The blue dots represent the radius of gyration (Rg) for the 300 µM sample. The left y axis is the scattering intensity from SAXS data, and the right y axis is the Rg as determined by an automated Guinier fit of each frame. The graph was generated by the SIBLYS beamline.

The data immediately after the first peak in the chromatogram (**Figure 3.13**) of the 150 µM was chosen for further analysis as it had a more consistent Rg of around 30 Å and appeared to have the best potential for a quality background subtraction. The Rg is shown as the blue dots, and it is illustrated more clearly in **Figure 3.14a** as the dots in the purple highlighted reach. Unfortunately, each sample had significant background following the initial elution peak, limiting our ability to assess the data significantly.

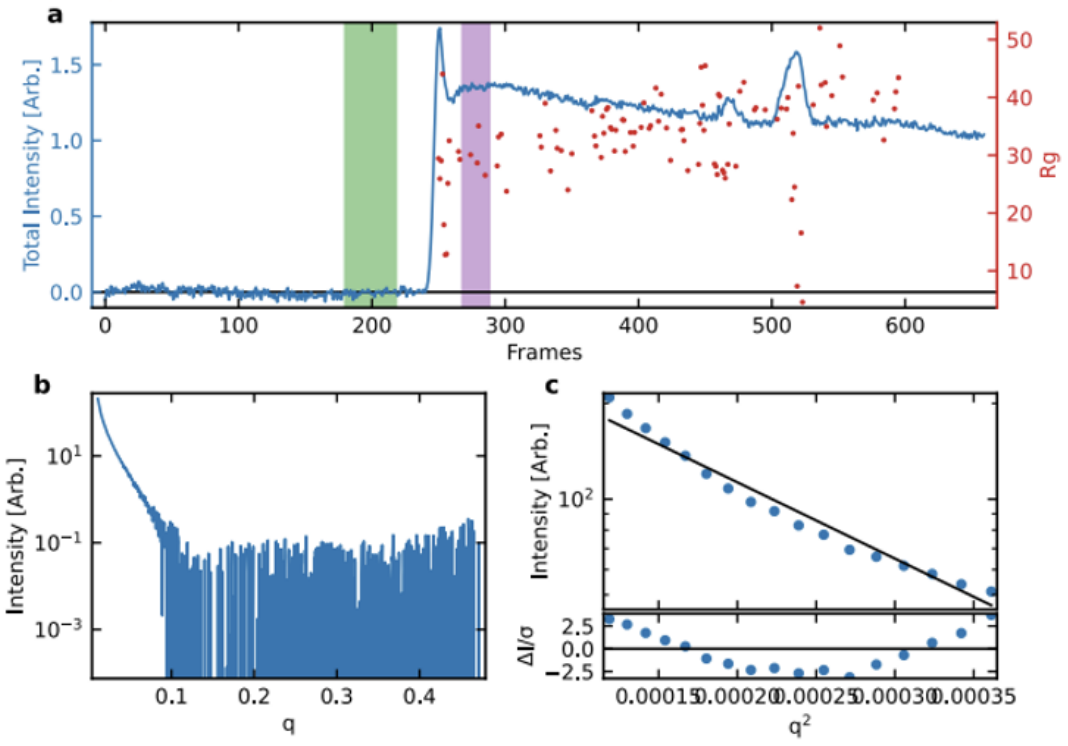

Figure 3.14: SEC-SAXS profile from the SIBLYS beamline. **(a)** Chromatogram of the data with the green band showing the region used for the buffer background, the purple band showing the data used for interpretation in b, c, d, and e, and the red dots show the Rg. **(b)** Scattering profile of SEC-SAXS data. **(c)** Guinier fit of the data along with the residual plot below.

The SEC-SAXS data was not able to be successfully subtracted because the background may have been too high or inconsistent as illustrated by significant background after the elution peak shown on the chromatogram. In **Figure 3.14a**, after the first elution peak, the *Rg* appears to be around 30 Å, but based on the Guinier fit of the averaged region, highlighted in **Figure 3.14c**, there may be interparticle interactions. The second elution peak, located right after 500 frames, is not usable due to the inconsistency of *Rg* and high background. Additionally, a linear fit is imposed on a Guinier region that is not linear, and the residual plot displays an upturn, all of which are indicative of potential non-specific aggregation, thus preventing the accurate estimation of *Rg* from these data. **Figure 3.14b** illustrates the buffer as over-subtracted, which can be seen by the signal

oscillating from 0 intensity to around an Intensity of around 0.1. The red dots on the graph are illustrating the *Rg*, which appears to be around 30 Å.

Double stranded DNA has a width of 20 Å, and if the oligonucleotide sequence was completely unfolded, it would have a length of 85 Å. Since the CD data for the RAD17 promoter sequence in HEPES at 1 mM lithium shows a clear i-motif structure, these SAXS measurements could be indicative of aggregation or potentially polymer i-motif fibers. There is very little in the literature of aggregation characteristics of i-motifs, but one application explaining the potential for i-motifs to aggregate is in i-motif nanowires. In a computational study with molecular dynamics, Singh *et al* 2013 found that i-motifs make unique nanowires in that they are much more flexible than other biological polymers, but they do exhibit more than 300 mPa of tensile strength.[91] While more detailed structural studies are needed to verify if the aggregation seen is a polymer i-motif fiber or rather non-specific aggregation, the literature reports of nanowires do suggest that more studies of i-motif association between i-motif units is needed. Furthermore, a more robust folding protocol could be developed to more specifically tune the aggregation response for i-motifs. Furthermore, additional SAXS studies are warranted to validate structural conclusions.

CHAPTER 4: CONCLUSION

I-motifs are a relatively newly discovered DNA structure that utilize non-canonical cytosine-cytosine base pairing to form a four stranded-intercalated structure. They are important as a pH dependent switch for a variety of biomedical applications, and they are biologically relevant due to their existence in the nucleus of living cells during the end of G1 and start of S in the cell cycle.[7, 36] However, due to their transient nature, much more research is needed to fully elucidate their role in biological processes such as transcription. Even with the current literature, however, there is disagreement on certain features of i-motifs, most notably which ions stabilize or de-stabilize their structure.

The present work aimed to address these issues, in part, by assessing the folding of a well-known i-motif forming oligonucleotide from the RAD17 promoter sequence in three buffers and with varying concentrations of two monovalent cations, sodium and lithium. The primary means of assessing the structural state of the oligo under investigation was via circular dichroism. Using CD, the alternative folding modes for this oligo, namely i-motifs and hairpins, could be distinguished as the major population in any given condition. Small-angle x-ray scattering was also used to assess the structure of this oligo in a lithium titration series.

The first part of this study examined which buffers formed i-motifs at physiological pH. Once it was established with circular dichroism that HEPES facilitated i-motif formation whereas tris-borate and tris acetate favored hairpin formation, HEPES was chosen as the buffer system moving forward to determine ion effects. In HEPES, lithium values at 1 mM and less had a clear i-motif present in the CD spectra, whereas higher concentrations favored hairpin formation. There are several theories in the literature as to how lithium exerts its therapeutic or toxic effects. Of all

the potential theories, the most interesting one that could be relevant to this research is that lithium has been shown to alter gene expression of some proteins such as CREB and p53, possibly through interfering with transcription, but more research is needed to understand how this may occur.[40]

With sodium, the transition was more gradual, and the spectral signatures were less definitive other than the 3 mM sodium which clearly demonstrated an i-motif. The sodium data suggest that there could be additional structural transitions occurring besides a clear i-motif to hairpin at certain critical titration points, as seen with lithium.

The final part of this study was to utilize SAXS to provide additional structural information about i-motifs. With HT SAXS, the scattering data was consistent with the CD data that the structure was most likely a hairpin due to the P(r) peak at 20 Å, and a Dmax of around 65 Å, that could be consistent with the short hairpin and long single stranded region predicted by NUPACK.

Buffer choice clearly has an effect on DNA structure, which could explain the contradictory reports of metal ion effects on i-motif stability, specifically for lithium and sodium. The next steps would be to elucidate what potential structural interactions are occurring and to do a more thorough follow-up on if the mechanism for tris promoting hairpin formation is due to buffer protonation and interaction with the phosphate backbone. That could be tested by increasing the pH, which would reduce the proportion of protonated tris species. If this led to more stable i-motif formation, this would help validate this potential mechanism. However, since i-motifs prefer an acidic pH, stabilizing factors such as polyethylene glycol would be needed to ensure the results are not skewed due to poor conditions for i-motif formation. Melting experiments would also be useful to determine not only which structures are predominate in the sample, but to also assess stability. Tris would likely not be a good candidate for the temperature studies because solutions containing tris can have a variable pH in response to temperature.[92]

Other research to better understand the biological significance of i-motifs would be to better mimic the cellular environment such as molecular crowding, and potentially do similar studies on other i-motif promoter regions. This would assist in providing a better overall picture of the i-motif's role in regulating transcription. For example, the serotonin transport gene (SERT) has been shown to form i-motifs, but the different allelic variants of SERT exhibit varying structural properties.[44] However, there is not currently further insight into what these structural differences are, nor is there a theory as to how these changes may impact depression. I-motif structural studies with SAXS, CD, and ion interactions could potentially enhance current understanding of mental illness.

More information is still needed to better understand the role that i-motifs play in transcription. BmILF, HNRNP LL, and BmPOUM2 are transcription factors known to bind i-motifs[18, 93], and research efforts by other groups are ongoing to discover more i-motif binding ligands.[94] In the BCL2 gene, HNRNP LL recognizes the distinct i-motif structure, and the binding initiates resolution of the i-motif structure, and transcription is upregulated.[18, 95] If the i-motif is already unfolded on non-existent, HNRNP LL is not able to bind, and as a result, transcription cannot occur. However, in the c-MYC promotor region, HNRNPK still recognizes and binds to i-motifs to activate transcription[18, 96], but persistent i-motif stability inhibits further transcription by blocking the sites for further transcriptional activity. It is also important to note that the i-motifs are a transient structure that are more likely to form in regions of negative super helicity as well as in the G1 phase of the cell cycle, which indicate that they could function to assist with getting cells ready for replication.[7, 10, 18, 95]

Another future study that would greatly aid in understanding the role of buffers in biological systems would be to conduct binding studies to determine under which conditions

buffers may act as a ligand to DNA or cations. Single-molecule FRET is a popular technique for studying i-motif binding interactions as well as folding and unfolding.[21] Determining how these molecules are interacting with each other would be pivotal in experimental design of biomolecules, and it would greatly enhance real-world applicability.

Overall, more thoughtful consideration of buffer choice when conducting research is important to making insightful observations that are not unintentionally skewed due to unforeseen variables. This is especially critically when making assumptions from research studies that aim ultimately to better understand or treat disease processes. Thus, all these deficiencies present in the current literature necessitate further research into i-motif structure and significance to physiological as well as pathological processes.

REFERENCES

(1) Li, Z. K.; Song, W. J.; Zhu, Y. H.; Yan, L.; Zhong, X.; Zhang, M. L.; Li, H. The Full Cytosine-Cytosine Base Paring: Self-Assembly and Crystal Structure. *Chemistry-a European Journal* **2023**. DOI: 10.1002/chem.202203979.
(2) Amato, J.; Iaccarino, N.; D'Aria, F.; D'Amico, F.; Randazzo, A.; Giancola, C.; Cesaro, A.; Di Fonzo, S.; Pagano, B. Conformational plasticity of DNA secondary structures: probing the conversion between i-motif and hairpin species by circular dichroism and ultraviolet resonance Raman spectroscopies. *Physical Chemistry Chemical Physics* **2022**, *24* (11), 7028-7044. DOI: 10.1039/d2cp00058j.
(3) Cui, Y. X.; Kong, D. M.; Ghimire, C.; Xu, C. X.; Mao, H. B. Mutually Exclusive Formation of G-Quadruplex and i-Motif Is a General Phenomenon Governed by Steric Hindrance in Duplex DNA. *Biochemistry* **2016**, *55* (15), 2291-2299. DOI: 10.1021/acs.biochem.6b00016.
(4) Manalastas-Cantos, K.; Konarev, P. V.; Hajizadeh, N. R.; Kikhney, A. G.; Petoukhov, M. V.; Molodenskiy, D. S.; Panjkovic, A.; Merten, H. D. T.; Gruzinov, A.; Borges, C.; et al. ATSAS 3.0: expanded functionality and new tools for small-angle scattering analysis. J. Appl. Cryst, 2021; Vol. 54, pp 343-355.
(5) Petoukhov, M. V.; Franke, D.; Shkumatov, A. V.; Tria, G.; Kikhney, A. G.; Gajda, M.; Gorba, C.; Mertens, H. D. T.; Konarev, P. V.; Svergun, D. I. New developments in the ATSAS program package for small-angle scattering data analysis. *Journal of Applied Crystallography* **2012**, *45*, 342-350, Software Review. DOI: 10.1107/s0021889812007662.
(6) Manalastas-Cantos, K.; Konarev, P. V.; Hajizadeh, N. R.; Kikhney, A. G.; Petoukhov, M. V.; Molodenskiy, D. S.; Panjkovich, A.; Mertens, H. D. T.; Gruzinov, A.; Borges, C.; et al. ATSAS 3.0: expanded functionality and new tools for small-angle scattering data analysis. J. Appl. Cryst., 2021; Vol. 54, pp 343-355.
(7) Abou Assi, H.; Garavís, M.; González, C.; Damha, M. J. i-Motif DNA: structural features and significance to cell biology. *Nucleic Acids Res* **2018**, *46* (16), 8038-8056. DOI: 10.1093/nar/gky735.
(8) Paul, S.; Hossain, S. S.; Samanta, A. Insights into the Folding Pathway of a c-MYC-Promoter-Based i-Motif DNA in Crowded Environments at the Single-Molecule Level. *J Phys Chem B* **2020**, *124* (5), 763-770. DOI: 10.1021/acs.jpcb.9b10633.
(9) Zeraati, M.; Langley, D. B.; Schofield, P.; Moye, A. L.; Rouet, R.; Hughes, W. E.; Bryan, T. M.; Dinger, M. E.; Christ, D. I-motif DNA structures are formed in the nuclei of human cells. *Nat Chem* **2018**, *10* (6), 631-637. DOI: 10.1038/s41557-018-0046-3.
(10) Bertoli, C.; Skotheim, J. M.; de Bruin, R. A. Control of cell cycle transcription during G1 and S phases. *Nat Rev Mol Cell Biol* **2013**, *14* (8), 518-528. DOI: 10.1038/nrm3629.
(11) Oh, K. I.; Kim, J.; Park, C. J.; Lee, J. H. Dynamics Studies of DNA with Non-canonical Structure Using NMR Spectroscopy. *Int J Mol Sci* **2020**, *21* (8). DOI: 10.3390/ijms21082673.
(12) Cui, J. J.; Waltman, P.; Le, V. H.; Lewis, E. A. The Effect of Molecular Crowding on the Stability of Human c-MYC Promoter Sequence I-Motif at Neutral pH. *Molecules* **2013**, *18* (10), 12751-12767. DOI: 10.3390/molecules181012751.
(13) Fleming, M. A.; Ding, Y.; Rogers, R. A.; Zhu, J.; Zhu, J.; Burton, A. D.; Carlisle, C. B.; Burrows, C. J. 4n-1 Is a "Sweet Spot" in DNA i-Motif Folding of 2'-Deoxycytidine Homopolymers. *American Chemical Society* **2017**, *139*, 7.

(14) Day, H. A.; Huguin, C.; Waller, Z. A. Silver cations fold i-motif at neutral pH. *Chem Commun (Camb)* **2013**, *49* (70), 7696-7698. DOI: 10.1039/c3cc43495h.
(15) Dong, Y.; Yang, Z.; Liu, D. DNA nanotechnology based on i-motif structures. *Acc Chem Res* **2014**, *47* (6), 1853-1860. DOI: 10.1021/ar500073a.
(16) Ma, W.; Sun, H.; Chen, B.; Jia, R.; Huang, J.; Cheng, H.; He, X.; Huang, M.; Wang, K. Engineering a Facile Aptamer "Molecule-Doctor" with Hairpin-Contained I-Motif Enables Accurate Imaging and Killing of Cancer Cells. *Anal Chem* **2021**, *93* (43), 14552-14559. DOI: 10.1021/acs.analchem.1c03580.
(17) Hu, Y.; Gao, S.; Lu, H.; Ying, J. Y. Acid-Resistant and Physiological pH-Responsive DNA Hydrogel Composed of A-Motif and i-Motif toward Oral Insulin Delivery. *J Am Chem Soc* **2022**, *144* (12), 5461-5470. DOI: 10.1021/jacs.1c13426.
(18) Brown, S. L.; Kendrick, S. The i-Motif as a Molecular Target: More Than a Complementary DNA Secondary Structure. *Pharmaceuticals (Basel)* **2021**, *14* (2). DOI: 10.3390/ph14020096.
(19) Radha, G.; Raghavan, S. C. BCL2: A promising cancer therapeutic target. *Biochimica Et Biophysica Acta-Reviews on Cancer* **2017**, *1868* (1), 309-314. DOI: 10.1016/j.bbcan.2017.06.004.
(20) Nguyen, L.; Papenhausen, P.; Shao, H. P. The Role of c-MYC in B-Cell Lymphomas: Diagnostic and Molecular Aspects. *Genes* **2017**, *8* (4). DOI: 10.3390/genes8040116.
(21) Kim, S. E.; Lee, I. B.; Hyeon, C.; Hong, S. C. Destabilization of i-Motif by Submolar Concentrations of a Monovalent Cation. *Journal of Physical Chemistry B* **2014**, *118* (18), 4753-4760. DOI: 10.1021/jp500120d.
(22) Mergny, J. L.; Lacroix, L.; Han, X. G.; Leroy, J. L.; Helene, C. INTRAMOLECULAR FOLDING OF PYRIMIDINE OLIGODEOXYNUCLEOTIDES INTO AN I-DNA MOTIF. *Journal of the American Chemical Society* **1995**, *117* (35), 8887-8898. DOI: 10.1021/ja00140a001.
(23) Gao, J. H.; Berden, G.; Rodgers, M. T.; Oomens, J. Interaction of Cu⁺ with cytosine and formation of i-motif-like C-M⁺-C complexes: alkali versus coinage metals. *Physical Chemistry Chemical Physics* **2016**, *18* (10), 7269-7277. DOI: 10.1039/c6cp00234j.
(24) Kohagen, M.; Uhlig, F.; Smiatek, J. On the nature of ion-stabilized cytosine pairs in DNA i-motifs: The importance of charge transfer processes. *International Journal of Quantum Chemistry* **2019**, *119* (14). DOI: 10.1002/qua.25933.
(25) Mustafa, G.; Gyawali, P.; Taylor, J. A.; Maleki, P.; Nunez, M. V.; Guntrum, M. C.; Shiekh, S.; Balci, H. A single molecule investigation of i-motif stability, folding intermediates, and potential as in-situ pH sensor. *Frontiers in Molecular Biosciences* **2022**, *9*, 12, Article. DOI: 10.3389/fmolb.2022.977113.
(26) Dhakal, S.; Yu, Z. B.; Konik, R.; Cui, Y. X.; Koirala, D.; Mao, H. B. G-Quadruplex and i-Motif Are Mutually Exclusive in ILPR Double-Stranded DNA. *Biophysical Journal* **2012**, *102* (11), 2575-2584. DOI: 10.1016/j.bpj.2012.04.024.
(27) Gao, B.; Hou, X. M. Opposite Effects of Potassium Ions on the Thermal Stability of i-Motif DNA in Different Buffer Systems. *Acs Omega* **2021**, *6* (13), 8976-8985. DOI: 10.1021/acsomega.0c06350.
(28) Saxena, S.; Joshi, S.; Shankaraswamy, J.; Tyagi, S.; Kukreti, S. Magnesium and molecular crowding of the cosolutes stabilize the i-motif structure at physiological pH. *Biopolymers* **2017**, *107* (7). DOI: 10.1002/bip.23018.

(29) Zhao, D. D.; Tang, H. R.; Wang, H.; Yang, C.; Li, Y. X. Analytes Triggered Conformational Switch of i-Motif DNA inside Gold-Decorated Solid-State Nanopores. *Acs Sensors* **2020**, *5* (7), 2177-2183. DOI: 10.1021/acssensors.0c00798.
(30) Shi, Y. H.; Sun, H. X.; Xiang, J. F.; Yu, L. J.; Yang, Q. F.; Li, Q.; Guan, A. J.; Tang, Y. L. i-Motif-modulated fluorescence detection of silver(I) with an ultrahigh specificity. *Analytica Chimica Acta* **2015**, *857*, 79-84. DOI: 10.1016/j.aca.2014.12.002.
(31) Day, H. A.; Wright, E. P.; MacDonald, C. J.; Gates, A. J.; Waller, Z. A. E. Reversible DNA i-motif to hairpin switching induced by copper(II) cations. *Chemical Communications* **2015**, *51* (74), 14099-14102. DOI: 10.1039/c5cc05111h.
(32) Miao, D. D.; Yu, Y. Y.; Chen, Y.; Liu, Y.; Su, G. X. Facile Construction of i-Motif DNA-Conjugated Gold Nanostars as Near-Infrared and pH Dual-Responsive Targeted Drug Delivery Systems for Combined Cancer Therapy. *Molecular Pharmaceutics* **2020**, *17* (4), 1127-1138. DOI: 10.1021/acs.molpharmaceut.9b01159.
(33) Huard, D. J. E.; Demissie, A.; Kim, D.; Lewis, D.; Dickson, R. M.; Petty, J. T.; Lieberman, R. L. Atomic Structure of a Fluorescent Ag₈ Cluster Templated by a Multistranded DNA Scaffold. *Journal of the American Chemical Society* **2019**, *141* (29), 11465-11470. DOI: 10.1021/jacs.8b12203.
(34) Yu, X.-M.; Groveman, B.; Fang, X.-Q.; Lin, S.-X. The role of intracellular sodium (Na^+) in the regulation of calcium ($Ca2^+$) mediated signaling and toxicity. *Health (Irvine Calif)* **2010**, *2*, 7.
(35) Wang, Y.; Demir, B.; Mohammad, H.; Oren, E. E.; Anantram, M. P. A computational study of the role of counterions and solvent dielectric in determining the conductance of B-DNA. *bioRxiv* **2023**.
(36) Dzatko, S.; Krafcikova, M.; Hänsel-Hertsch, R.; Fessl, T.; Fiala, R.; Loja, T.; Krafcik, D.; Mergny, J. L.; Foldynova-Trantirkova, S.; Trantirek, L. Evaluation of the Stability of DNA i-Motifs in the Nuclei of Living Mammalian Cells. *Angewandte Chemie-International Edition* **2018**, *57* (8), 2165-2169. DOI: 10.1002/anie.201712284.
(37) Dick, D. The distribution of sodium, potassium and chloride in the nucleus and cytoplasm of BUFO BUFO oocytes measured by electron microprobe analysis. *J. Physiol.* **1978**, *284*, 37-53.
(38) Strazzullo, P.; Leclercq, C. Sodium. *Advances in Nutrition* **2014**, *5* (2), 188-190. DOI: 10.3945/an.113.005215.
(39) Folkerd, E.; Singer, D. R. J.; Cappuccio, F. P.; Markandu, N. D.; Sampson, B.; Macgregor, G. A. CLEARANCE OF ENDOGENOUS LITHIUM IN HUMANS - ALTERED DIETARY SALT INTAKE AND COMPARISON WITH EXOGENOUS LITHIUM CLEARANCE. *American Journal of Physiology-Renal Fluid and Electrolyte Physiology* **1995**, *268* (4), F718-F722. DOI: 10.1152/ajprenal.1995.268.4.F718.
(40) Alda, M. Lithium in the treatment of bipolar disorder: Pharmacology and pharmacogenetics. *Mol Psychiatry* **2015**, *20* (6), 661-670.
(41) Altschul, E.; Grossman, C.; Dougherty, R.; Gaikwad, R.; Nguyen, V.; Schwimmer, J.; Merker, E.; Mandel, S. Lithium Toxicity: A Review of Pathophysiology, Treatment, and Prognosis. *Practical Neurology* **2016**, *15* (2).
(42) MacLeod-Glover, N.; Chuang, R. Chronic lithium toxicity Considerations and systems analysis. *Canadian Family Physician* **2020**, *66* (4), 258-261.
(43) Gunawan, R.; Imran, A.; Ahmed, I.; Liu, Y. C.; Chu, Y. W.; Guo, L. B.; Yang, M. S.; Lau, C. FROZEN! Intracellular multi-electrolyte analysis measures millimolar lithium in mammalian cells. *Analyst* **2021**, *146* (16), 5186-5197. DOI: 10.1039/d1an00806d.

(44) Thorne, B. N.; Ellenbroek, B. A.; Day, D. J. Evaluation of i-Motif Formation in the Serotonin Transporter-Linked Polymorphic Region. *Chembiochem* **2021**, *22* (2), 349-353. DOI: 10.1002/cbic.202000513.
(45) Minasyan, A. S.; Chakravarthy, S.; Vardelly, S.; Joseph, M.; Nesterov, E. E.; Nesterova, I. V. Rational design of guiding elements to control folding topology in i-motifs with multiple quadruplexes. *Nanoscale* **2021**, *13* (19), 8875-8883. DOI: 10.1039/d1nr00611h.
(46) Rogers, R. A.; Fleming, A. M.; Burrows, C. J. Rapid Screen of Potential i-Motif Forming Sequences in DNA Repair Gene Promoters. *ACS Omega* **2018**, *3* (8), 9630-9635. DOI: 10.1021/acsomega.8b01551.
(47) Lloret-Llinares, M.; Karadoulama, E.; Chen, Y.; Wojenski, L. A.; Villafano, G. J.; Bornholdt, J.; Andersson, R.; Core, L.; Sandelin, A.; Jensen, T. H. The RNA exosome contributes to gene expression regulation during stem cell differentiation. *Nucleic Acids Research* **2018**, *46* (21), 11502-11513. DOI: 10.1093/nar/gky817.
(48) Hopkins, E.; Sanvictores, T.; Sharma, S. *Physiology, Acid Base Balance*; StatPearls Publishing, 2022.
(49) Shen, J. B.; Zeng, Y. L.; Zhuang, X. H.; Sun, L.; Yao, X. Q.; Pimpl, P.; Jiang, L. W. Organelle pH in the Arabidopsis Endomembrane System. *Molecular Plant* **2013**, *6* (5), 1419-1437. DOI: 10.1093/mp/sst079.
(50) Herlihy, A. E.; de Bruin, R. A. M. The Role of the Transcriptional Response to DNA Replication Stress. *Genes* **2017**, *8* (3). DOI: 10.3390/genes8030092.
(51) Kypr, J.; Kejnovská, I.; Renciuk, D.; Vorlícková, M. Circular dichroism and conformational polymorphism of DNA. *Nucleic Acids Res* **2009**, *37* (6), 1713-1725. DOI: 10.1093/nar/gkp026.
(52) Kypr, J.; Kejnovská, I.; Bednárová, K.; Vorlíčková, M. Circular Dichroism Spectroscopy of Nucleic Acids. *Comprehensive Chiroptical Spectroscopy* **2012**, *2*, 11.
(53) Bishop, G. R.; Chaires, J. B. Characterization of DNA Structures by Circular Dichroism. *Current protocols in nucleic acid chemistry* **2003**, *11* (1), 7.
(54) Miyahara, T.; Nakatsuji, H.; Sugiyama, H. Helical Structure and Circular Dichroism Spectra of DNA: A Theoretical Study. *Journal of Physical Chemistry A* **2013**, *117* (1), 42-55. DOI: 10.1021/jp3085556.
(55) Hurlburt, N. *Circular Dichroism*. 2022. https://chem.libretexts.org/Bookshelves/Physical_and_Theoretical_Chemistry_Textbook_Maps/Supplemental_Modules_(Physical_and_Theoretical_Chemistry)/Spectroscopy/Electronic_Spectroscopy/Circular_Dichroism (accessed 2022 April 10, 2022).
(56) Johnson, C. *Circular Dichroism and the Conformational Analysis of Biomolecules*; Springer, 1996.
(57) Jacques, D.; Trewhella, J. Small-angle scattering for structural biology-Expanding the frontier while avoiding the pitfalls. *Protein Science* **2010**, *19* (4), 642-657, Review. DOI: 10.1002/pro.351.
(58) Burke, J. E.; Butcher, S. E. Nucleic acid structure characterization by small angle X-ray scattering (SAXS). *Curr Protoc Nucleic Acid Chem* **2012**, *Chapter 7*, Unit7.18. DOI: 10.1002/0471142700.nc0718s51.
(59) Oliver, R. C.; Rolband, L. A.; Hutchinson-Lundy, A. M.; Afonin, K. A.; Krueger, J. K. Small-Angle Scattering as a Structural Probe for Nucleic Acid Nanoparticles (NANPs) in a Dynamic Solution Environment. *Nanomaterials (Basel)* **2019**, *9* (5). DOI: 10.3390/nano9050681.

(60) Weiss, T. M. Small Angle Scattering: Historical Perspective and Future Outlook. In *Biological Small Angle Scattering: Techniques, Strategies and Tips*, Chaudhuri, B., Munoz, I. G., Qian, S., Urban, V. S. Eds.; Advances in Experimental Medicine and Biology, Vol. 1009; Springer-Verlag Singapore Pte Ltd, 2017; pp 1-10.
(61) Chen, Y.; Pollack, L. SAXS studies of RNA: structures, dynamics, and interactions with partners. *Wiley Interdiscip Rev RNA* **2016**, *7* (4), 512-526. DOI: 10.1002/wrna.1349.
(62) Boldon, L.; Laliberte, F.; Liu, L. Review of the fundamental theories behind small angle X-ray scattering, molecular dynamics simulations, and relevant integrated application. *Nano reviews* **2015**, *6*, 25661. DOI: 10.3402/nano.v6.25661.
(63) Trewhella, J.; Nakamura, H.; Kleywegt, G.; Burley, S.; Markley, J. Small Angle Scattering and Structural Biology: Data Quality and Model Validation. *Integrative Structural Biology With Hybrid Methods* **2018**, *1105*, 77-100, Article|Book Chapter. DOI: 10.1007/978-981-13-2200-6_7.
(64) Putnam, C. Guinier peak analysis for visual and automated inspection of small-angle X-ray scattering data. *Journal of Applied Crystallography* **2016**, *49*, 1412-1419, Article. DOI: 10.1107/S1600576716010906.
(65) Komori, K.; Sakae, S.; Shinagawa, H.; Morikawa, K.; Ishino, Y. A Holliday junction resolvase from Pyrococcus furiosus:: Functional similarity to Escherichia coli RuvC provides evidence for conserved mechanism of homologous recombination in Bacteria, Eukarya, and Archaea. *Proceedings of the National Academy of Sciences of the United States of America* **1999**, *96* (16), 8873-8878. DOI: 10.1073/pnas.96.16.8873.
(66) *CD Sample Preparation*. Vanderbilt, 2014. https://structbio.vanderbilt.edu/wetlab/cd.sample.prep.php (accessed 2022 April 8, 2022).
(67) *Tris-Cl*. Cold Spring Harbor Protocols, 2006. https://cshprotocols.cshlp.org/content/2006/1/pdb.rec8063.short#:~:text=The%20pH%20of%20Tris%20solutions,and%2037%C2%B0C%2C%20respectively. (accessed 2023.
(68) Luo, S. H.; Pal, D.; Shah, S. J.; Kwatra, D.; Paturi, K. D.; Mitra, A. K. Effect of HEPES Buffer on the Uptake and Transport of P-Glycoprotein Substrates and Large Neutral Amino Acids. *Molecular Pharmaceutics* **2010**, *7* (2), 412-420. DOI: 10.1021/mp900193e.
(69) MODEL J-715
Spectropolarimeter
Hardware Manual
Jasco: Jasco, 1995.
(70) *Circular Dichroism (Overview)*. Jasco, 2017. https://jascoinc.com/learning-center/theory/spectroscopy/circular-dichroism-spectroscopy/ (accessed 2022 April 28, 2022).
(71) J-800 Series
CD Spectrometer
Software Operation Manual
Spectra Manager Ver. 2. Jasco: Jasco, 2007.
(72) Fornace, M. E.; Huang, J.; Newman, C. T.; Porubsky, N. J.; Pierce, M. B.; Pierce, N. A. NUPACK: analysis and design of nucleic acid structures, devices, and systems. ChemRxiv: 2022.
(73) Zadeh, J. N.; Steenberg, C. D.; Bois, J. S.; Wolfe, B. R.; Pierce, M. B.; Khan, A. R.; Dirks, R. M.; Pierce, N. A. NUPACK: analysis and design of nucleic acid systems. J Comput Chem, 2011; Vol. 32, pp 170-173.

(74) Singhal, H.; Ren, Y. Z. R.; Kern, S. E. Improved DNA Electrophoresis in Conditions Favoring Polyborates and Lewis Acid Complexation. *Plos One* **2010**, *5* (6). DOI: 10.1371/journal.pone.0011318.
(75) Spear, N.; Aust, S. D. The Effects of Different Buffers on the Oxidation of DNA by Thiols and Ferric Iron. *Journal of Biochemical and Molecular Toxicology* **1998**, *12* (2), 125-132. DOI: 10.1002/(sici)1099-0461(1998)12:2<125::aid-jbt7>3.0.co;2-n.
(76) Stellwagen, N. C.; Bossi, A.; Gelfi, C.; Righetti, P. G. DNA and buffers: Are there any noninteracting, neutral pH buffers? *Analytical Biochemistry* **2000**, *287* (1), 167-175. DOI: 10.1006/abio.2000.4848.
(77) YazdanYar, A.; Buswell, L.; Pantaloni, D.; Aschauer, U.; Bowen, P. Interaction of Tris with rutile surfaces and consequences for *in vitro* bioactivity testing. *Open Ceramics* **2021**, *7*.
(78) *PubChem Compound Summary for CID 23831, 4-(2-Hydroxyethyl)-1-piperazine ethanesulfonic acid*. NIH, https://pubchem.ncbi.nlm.nih.gov/compound/hepes (accessed 2023.
(79) Mohan, C. *Buffers A guide for the preparation and use of buffers in biological systems*. 2006. https://www.med.unc.edu/pharm/sondeklab/wp-content/uploads/sites/868/2018/10/buffers_calbiochem.pdf (accessed 2023 11/15/2023).
(80) El Balkhi, S.; Megarbane, B.; Poupon, J.; Baud, F.; Galliot-Guilley, M. Lithium poisoning: Is determination of the red blood cell lithium concentration useful? *Clinical Toxicology* **2009**, *47* (1), 8-13. DOI: 10.1080/15563650802392398.
(81) Fleysher, L.; Oesingmann, N.; Brown, R.; Sodickson, D.; Wiggins, G.; Inglese, M. Non-invasive Quantification of Intracellular Sodium in Human Brain using Ultra-High-Field MRI. *NMR Biomed* **2013**, *26* (1), 9-19.
(82) Pandiscia, L. Circular Dichroism Seminar. Jasco: Jasco, 2017.
(83) Marcus, Y. IONIC-RADII IN AQUEOUS-SOLUTIONS. *Chemical Reviews* **1988**, *88* (8), 1475-1498. DOI: 10.1021/cr00090a003.
(84) Yang, K. L.; Yiacoumi, S.; Tsouris, C. Monte Carlo simulations of electrical double-layer formation in nanopores. *Journal of Chemical Physics* **2002**, *117* (18), 8499-8507. DOI: 10.1063/1.1511726.
(85) Hayamizu, K.; Chiba, Y.; Haishi, T. Dynamic ionic radius of alkali metal ions in aqueous solution: a pulsed-field gradient NMR study. *Rsc Advances* **2021**, *11* (33), 20252-20257. DOI: 10.1039/d1ra02301b.
(86) Sims, P. A.; Wong, C. F.; Vuga, D.; McCammon, J. A.; Sefton, B. M. Relative contributions of desolvation, inter- and intramolecular interactions to binding affinity in protein kinase systems. *Journal of Computational Chemistry* **2005**, *26* (7), 668-681. DOI: 10.1002/jcc.20207.
(87) Hopkins, J. B.; Gillian, R. E.; Skou, S. BioXTAS RAW: improvements to a free open-source program for small-angle X-ray scattering data reduction and analysis. Journal of Applied Crystallography, 2017; Vol. 50, pp 1545-1553.
(88) Rolband, L.; Chopra, K.; Chandler, M.; Danai, L.; Beasock, D.; Krueger, J.; Byrnes, J.; Afonin, K. SAXS for NANPs: Advancing the structural characterization of nucleic acid nanoparticles through small-angle x-ray scattering. *Journal of Biological Chemistry* **2023**, *299* (3), S75-S75. DOI: 10.1016/j.jbc.2023.103208.
(89) Svergun, D. I. DETERMINATION OF THE REGULARIZATION PARAMETER IN INDIRECT-TRANSFORM METHODS USING PERCEPTUAL CRITERIA. *Journal of Applied Crystallography* **1992**, *25*, 495-503. DOI: 10.1107/s0021889892001663.

(90) Mirsaidov, U.; Comer, J.; Dimitrov, V.; Aksimentiev, A.; Timp, G. Slowing the translocation of double-stranded DNA using a nanopore smaller than the double helix. *Nanotechnology* **2010**, *21* (39). DOI: 10.1088/0957-4484/21/39/395501.
(91) Singh, R. P.; Blossey, R.; Cleri, F. Structure and Mechanical Characterization of DNA i-Motif Nanowires by Molecular Dynamics Simulation. *Biophysical Journal* **2013**, *105* (12), 2820-2831. DOI: 10.1016/j.bpj.2013.10.021.
(92) *Tris-HCl, 1 M Stock Solution, pH 7.80*. Sigma, https://www.sigmaaldrich.com/deepweb/assets/sigmaaldrich/product/documents/241/447/t2913dat.pdf (accessed 2023 November 22, 2023).
(93) Kang, H. J.; Kendrick, S.; Hecht, S. M.; Hurley, L. H. The Transcriptional Complex Between the BCL2 i-Motif and hnRNP LL Is a Molecular Switch for Control of Gene Expression That Can Be Modulated by Small Molecules. *Journal of the American Chemical Society* **2014**, *136* (11), 4172-4185. DOI: 10.1021/ja4109352.
(94) Wang, Y. H.; Yang, Q. F.; Lin, X.; Chen, D.; Wang, Z. Y.; Chen, B.; Han, H. Y.; Chen, H. D.; Cai, K. C.; Li, Q.; et al. G4LDB 2.2: a database for discovering and studying G-quadruplex and i-Motif ligands. *Nucleic Acids Res* **2022**, *50* (D1), D150-D160. DOI: 10.1093/nar/gkab952.
(95) Zanin, I.; Ruggiero, E.; Nicoletto, G.; Lago, S.; Maurizio, I.; Gallina, I.; Richter, S. N. Genome-wide mapping of i-motifs reveals their association with transcription regulation in live human cells. *Nucleic Acids Research* **2023**, *51* (16), 8309-8321. DOI: 10.1093/nar/gkad626.
(96) Shu, B.; Cao, J. J.; Kuang, G. T.; Qiu, J.; Zhang, M. L.; Zhang, Y.; Wang, M. X.; Li, X. Y.; Kang, S. S.; Ou, T. M.; et al. Syntheses and evaluation of new acridone derivatives for selective binding of oncogene c-myc promoter i-motifs in gene transcriptional regulation. *Chemical Communications* **2018**, *54* (16), 2036-2039. DOI: 10.1039/c8cc00328a.

APPENDIX A: SUPPLEMENTAL FIGURES

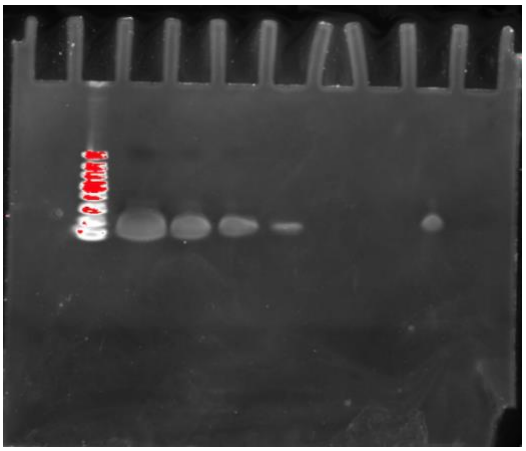

Supplemental Figure 1: 8% Urea PAGE of unpurified RAD17. Well 1: DNA Ladder, Well 2: 10µL DNA, Well 3: 5µL DNA, Well 4: 3µL DNA, Well 5: 1µL DNA. The DNA ladder is the called the "Ultra Low Range DNA Ladder", and the top band is 300 nucleotides, and the bottom band is 10 nucleotides.

The gel shown in Supplemental Figure 1 is demonstrating that the synthetic DNA oligonucleotide was reasonably pure and free of aggregates.

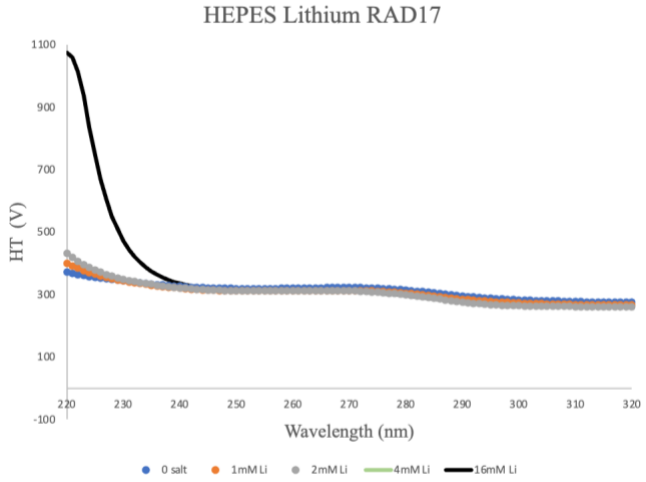

Supplemental Figure 2: HT voltage graph of RAD17 in HEPES**.** This HT voltage graph illustrates that there is not a significant change in HT voltage until the 16mM Lithium concentration, and that is limited to below 235nm. This indicates that especially for the 16mM Li concentration, the spectra below 240nm cannot be appropriately interpreted.

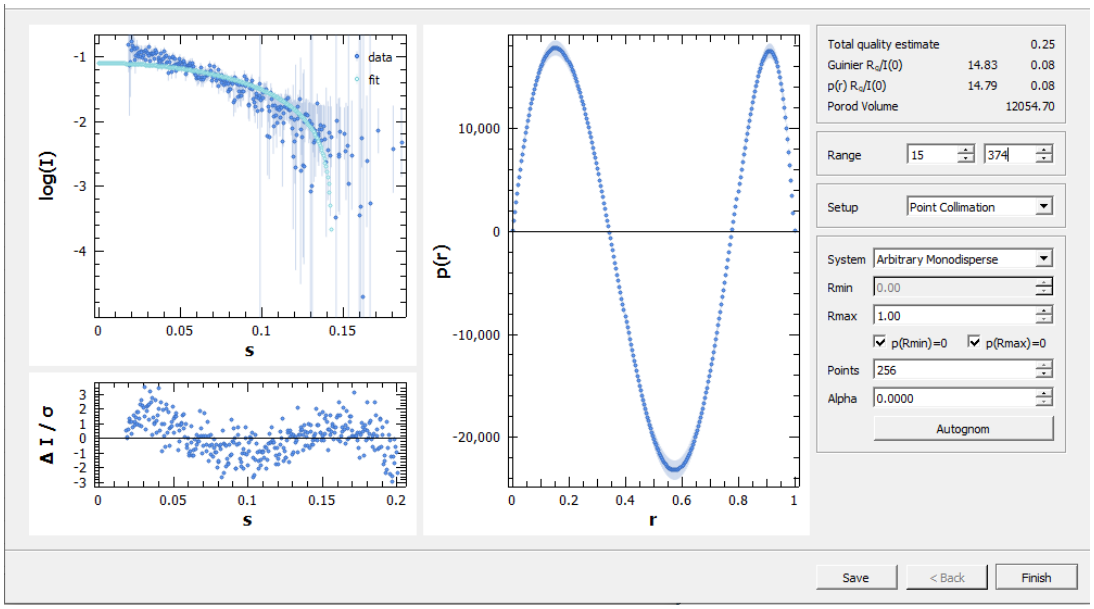

Supplemental Figure 3: 4mM Lithium sample. This figure is included to illustrate what noisy data from low sample concentration looks like. Data was plotted with ATSAS.[4]